UNIVERSITÀ DELLA CALABRIA

**UNIVERSITA' DELLA CALABRIA**

Dipartimento di Informatica, Modellistica, Elettronica e Sistemistica

**Dottorato di Ricerca in**

Ingegneria dei Sistemi ed Informatica

*Con il contributo del Dipartimento di Difesa del Suolo dell'Università della Calabria, nell'ambito del progetto PON01_01503: "Sistemi integrati per il monitoraggio, l'early warning e la mitigazione del rischio idrogeologico lungo le grandi vie di comunicazione".*

**XXVII CICLO**

# COMPACT AND WIDEBAND ANTENNAS FOR RADAR APPLICATIONS

**Settore Scientifico Disciplinare ING INF/02**

**Coordinatore:** Ch.mo Prof. SERGIO GRECO

Firma _____

**Supervisore/Tutor:** Ch.ma Prof.ssa SANDRA COSTANZO

Firma _____

**Dottorando:** Dott. ANTONIO COSTANZO

Firma _____

ANTONIO COSTANZO

# COMPACT AND WIDEBAND ANTENNAS FOR RADAR APPLICATIONS

October 2014

Developed in the framework of the project *PON 01-01503, Landslides Early Warning*

*To my Grandfather Pietro,*
*who learned me to look around.*

## Acknowledgements

To my supervisor Prof. Sandra Costanzo. She puts a lot of effort into trying to make me a good researcher.

To Prof. Giuseppe Di Massa, Mr. Ennio Marozzo and the staff of Microwave Laboratory. I learned a lot from you-all.

To Francesco, for his everlasting friendship and to Antonio, for his irreplaceable and omnipresent support.

To all my friends. The time we spent together made me a better person.

To my family...
homeland of my heart
and temple of my spirit.

To all the people believing in Science.

*Antonio*

# Preface

This work provides novel antenna designs and implementation techniques, in which the main goal is the satisfaction of strict requirements necessary for their integration in modern radar systems.

Modern radars, especially the ones used in sounder applications, work in the microwave frequency range. In particular, low frequencies are suitable for early warning applications and in each system needing a long range tracking. The most important motivation concerns the attenuation of the power associated to the signal during the path between radar and targets and vice versa; the attenuation, in general, increases with the frequency of the signal transmitted by the radar. However, the use of low frequencies, e.g. P-Band or L-Band frequency ranges, entails the employment of large antennas which dramatically waste the compactness, the practicality and the costs of the entire system, especially when the constraints require a very narrow beam, achievable only with an array composed by a large number of elements. An excessive weight of the antenna system causes a significant over-evaluating of the pointing system (engines, adapters, etc.) and protection structures for avoiding damages related to atmospheric agents, with additive costs.

In the emerging trend of software defined radar systems, most of the operations are delegated to software modules; this approach significantly stress classical drawbacks, as the versatility of the whole radar is mainly influenced by few hardware components, especially by the antenna device. An important aspect about the design of antennas for radar applications is related to the available bandwidth of the operations. Improving the bandwidth of the system means improving its resolution, so the use of a narrow band antenna often represents a significant bottleneck for the entire radar device. Unfortunately, antennas fabricated in microstrip technology, which probably are the most suitable in terms of costs and versatility, classically perform a few percent bandwidth; most of the techniques used to enlarge the bandwidth of a microstrip patch antenna deteriorate the behaviour in terms of radiation pattern, especially to the ratio of co-polar and cross-polar field components, symmetry of the field and gain.

So, the main aim of this research is to provide novel structures and techniques which assure a good trade-off between all these features, but maintaining low costs and easy designs.

The first structure proposed in this work has been designed starting by modifying the well known U-slotted Patch Antenna, one of the most-used design techniques in the recent literature. The novel structure has been produced in order to easy achieve a better compromise between large bandwidth, compactness of the device and quality of the radiation pattern. A mathematical model has been developed in order to find the correct geometrical parameters of the antenna and some prototypes for radar applications have been fabricated and tested in the Microwave Lab at University of Calabria, Italy.

The second structure proposed in this research is based on simplifying the geometrical features of the first one, in order to achieve almost the same behaviour but applying a simpler design. In this case two different prototype have been developed, fabricate and tested in our laboratory; the first prototype has been integrated in a radar system developed in the European Project $PON01 - 01503$, whose aim is the prevention, the early warning and the analysis of landslides, while the second one, developed with a novel scheme for a dual polarized antenna, has been integrated in a multi-mode and multi-frequency airborne radar system, developed by the research team CoRiSTA ( Consorzio di Ricerca sui TeleSensori Avanzati), under the supervision of the Italian Space Agency.

A bandwidth enlargement of the radar antenna, according to a significant size reduction, is the main goal also for the third structure here proposed, which is composed of a modified Fabry Perot Cavity Antenna fed by a rectangular wave-guide. In this case, a double layer structure composed of patches on a dielectric slab, acting as a meta-material, has been used to flatten the phase profile on the cavity screen, achieving a bandwidth several times larger than most of the ones already existing in literature. In particular, a novel synthesis technique mixing equivalent transmission line approach, method of moments and paraxial approximation of the wave equation in open resonators has been developed. A validation of this method, using both FEM and MoM full wave simulation analysis, has been performed and compared to the performance of similar structures.

# Sommario

Il lavoro di ricerca ha inizialmente riguardato il raffinamento di una configurazione di antenna a microstriscia da noi proposta, basata sull′utilizzo di un doppio sistema di fenditure nell′elemento radiante. La prima fenditura, a corona circolare, è posta intorno al punto di alimentazione, la seconda, invece, è assimilabile ad una U modificata. L′antenna presenta una buona banda di funzionamento, dimensioni ridotte rispetto al patch classico ed un buon comportamento in termini di riduzione della componente cross-polare. Partendo dai modelli matematici esistenti per la configurazione con slot ad U semplice, si è proposto un modello empirico per questa nuova tipologia di antenna, con il quale sono stati progettati, realizzati e testati due prototipi a banda larga, uno in banda P ed uno in banda C. La fenditura a corona circolare è stata inoltre utilizzata come base di una versione semplificata dellantenna, dimostrando una buona estensione di questa tecnica anche per antenne a doppia polarizzazione. Un primo prototipo a polarizzazione verticale, composto da una schiera 8x4 di elementi in banda L, è stato realizzato ed integrato in un modulo radar atto a rilevare le frane (Landslides Early Warning Radar Module). Un secondo prototipo, operante a 450MHz e sostanzialmente identico al primo, è stato utilizzato per un radar a multifrequenza sviluppato dal Consorzio di Ricerca sui Sistemi di Telesensori Avanzati (CORISTA). Per lo stesso radar, inoltre, è stato progettato un prototipo innovativo a doppia polarizzazione, usando come base lo stesso schema, operante in questo caso ad una frequenza di 900 MHz. Sia le misure, sia i test in volo, hanno confermato le performance di tutte le antenne progettate. L′ultima parte della ricerca ha prodotto una tecnica di sintesi anche per le antenne per applicazioni radar basate sui risuonatori Fabry Perot. La tecnica proposta riguarda la sintesi di metasuperfici a due strati che mostrano un andamento piatto della fase del coefficiente di riflessione in una banda molto ampia. Questa struttura, di dimensioni nettamente minori rispetto a tutte le altre presenti in letteratura, è stata quindi utilizzata per progettare un′antenna Fabry Perot con una banda molto più larga rispetto alla normale configurazione.

# Contents

# List of Figures

# List of Tables

# 1

# Modified U-Slotted Antenna

## 1.1 Introduction

Microstrip antennas, shortly described in Section 1.2, are widely used in the field of radar technology since many years due to their inherent advantages in terms of low cost, small size, easy integration and low profile characteristics [1]. However, the intrinsically narrow impedance bandwidth, caused by surface wave losses, strongly limits their application for modern radar systems, where multiband and/or broadband operations [2, 3, 4, 5, 6] are required to guarantee high data rate, while preserving at the same time the structure compactness [7, 8]. Various approaches have been proposed in literature to improve the bandwidth of standard patch antennas, such as the adoption of thicker substrates with low permittivity, the use of multi-layer and/or coplanar [9] configurations, based on the inclusion of parasitic elements above or around the primary radiator [10], which however causes an enlargement of the structure in the thickness or lateral direction [11]. An interesting single-layer configuration which preserves the thin profile characteristics of a standard microstrip patch, while assuring wideband and/or multiband operations, is based on the use of a coaxially fed rectangular patch with a U-shaped slot. First introduced in [12], it has been extensively studied in literature [12, 13, 14], with claimed impedance bandwidths in excess of 30 % for air substrate thickness of about 0.08 o ad in excess of 20 % for microwave substrates of similar thickness [15]. A description of the U-Slot Antenna is given in section 1.3. The basic idea of U-slot patch antenna is to exploit the reactive cancellation between the U-slot capacitance and the feed inductance, as well as the additional U-slot resonances, to obtain a broadband frequency response. Wide impedance bandwidths have been demonstrated for both linear and circular polarization [16], with a larger frequency band in the presence of an air or foam substrate, however a high cross-polar radiation has been also observed due to the complex combination of U-slot and patch resonant modes [17, 18].

Approximate formulas have been introduced [18] for the ratios between the vertical and the horizontal U-slot arms, as well as between the vertical U-slot

arm and the patch width, however high cross-polar levels have been observed at the same frequencies, even if satisfying these design rules. As a matter of fact, the major drawback of U-slot patch configuration is the strong sensitivity of the antenna behavior to the variation of different parameters describing the antenna geometry and the substrate. In this configuration, the currents on the patch surface cannot be separated into pure modes of either the slot or the patch, so each parameter variation causes a change in all resonant frequencies and could dramatically modify the antenna behavior [18]. Most of existing papers treat the design of U-slot configuration on the basis of numerical simulations which however precludes an easy process repeatability and a frequency scaling of the prototype. The finite-difference time domain method is adopted in [12], with the near-field to far-field transform [19, 20, 21, 22] applied to obtain the far-field radiation pattern. At the authors knowledge, the only significant attempt to establish design criteria for the U-slot patch configuration is reported in [18], where empirical formulas are presented on the basis of an accurate analysis of all structure resonances and their relations with the geometry parameters. However, design rules proposed in [18] give an approximate tool which may not work in all situations, and provide only a good starting point for successive optimization to be performed for achieving the prescribed broadband features. Starting from the insight study of the antenna behavior described in [18], the original U-slot geometry we propose in section 1.4 is properly modified to accomplish for a wideband response, but reducing cross-polarization effects due to the complex combination of the antenna and the slot modes. Cross-polarization levels represent a critical aspect for the design of broadband antennas, especially for the ones composed by single layer radiating elements, because unwanted higher-order modes excitation dramatically increase polarization impurity. High cross polarization not only leads to a distortion in the co-polarization pattern, but also reduces the gain of the antenna. A significant work was provided in [23], where a design for a dual L-strip lines exciting a triangular patch antenna, to obtain a wide operating bandwidth with cross-polarization level reduction, was presented In [24] a novel meandering probe was used to fed a wideband patch antenna on a thick substrate. Even if these technique are very effective on decreasing the cross-polar level on a wide band, feed designs lead to complicated structure, losing the compactness and easy feasibility that usually characterize microstrip patch antennas. A truncated ground-plane has been employed in [25], while a novel corner-fed microstrip square patch antenna, working at millimetre frequencies, is presented in [26], where surface currents have been studied to reduce the cross polarization components without complicating the design. However, in this case, bandwidth has been prominently sacrificed to improve differences between co-polar and cross-polar levels. In our work, a single layer slotted radiating element has been employed, without complication due to particular feed design or ground-plane, in order to maintain a high level of practicality, feasibility and robustness, which represent fundamental aspects in several scenarios, like in radar applications. Maintaining the complexity of

the design only on the radiating element allowed to find simple formulas for dimensioning all the geometrical parameters, avoiding further optimizations on the structure to decrease cross-polar levels. As a matter of fact, the modified U-shaped slot is introduced to properly minimize the unwanted currents giving rise to cross-polar radiation. As a further improvement with respect to the study presented in [18], the problem of thick substrates, usually required to satisfy bandwidth requirements in those applications such as P-sounding radar, is properly considered in this section.

The problem of large inductance due to the presence of a longer probe is accurately faced by adopting a proper annular gap around the coaxial feed, in order to reach a good impedance matching in the broad frequency range. Preliminary results have been discussed in [27, 28], an extensive theoretical discussion with a detailed description of the design rules derived for the antenna synthesis is presented in Section 1.4, with numerical validations at various frequencies up to 10 GHz. Finally, experimental results on compact P-band and C-band prototypes are discussed in Section 1.5 in order to demonstrate the effectiveness of the proposed approach.

## 1.2 Microstrip Antennas

Microstrip antenna was first introduced in the 1950s, with the earliest studies carried out by Grieg and Englemann [29], and by Deschamp [30]. However, the first successful results started to appear only 20 years later, when Byron described conducting strip radiators separated from a ground-plane by a dielectric substrate [31] and Munson patented the first microstrip antenna element [32]. In 80s, microstrip patch antennas were becoming much more widely known and used in a variety of communication systems. Since then, this class of antennas has been the subject of intensive research and development, so a particular attention was paid to improving mathematical models suitable for the design of the devices. Nowadays, there are several thousand papers published on the subject, as well as a number of books.

A basic microstrip antenna is composed by a metallic element supported above a large metallic ground plane by a thin dielectric substrate.The substrate thickness for the basic geometry is in the range of 0.01 to 0.05 free-space wavelengths. The dielectric constants of substrates are usually chosen in a range 1 to 10; for achieving low permittivity, air, polystyrene foam, or dielectric honeycomb are mostly employed, while ceramic or quartz based materials are usually chosen for their high values of permittivity . Common substrates used for microwave antenna design are provided in Tab. 1.1.

Dielectric constant is the ratio of the amount of electrical energy stored in an insulator, when a static electric field is imposed across it, relative to vacuum. A high dielectric constant will result in a smaller patch size which is good in most circuits though it will result in tighter fabrication tolerances. A high dielectric constant generally reduce the bandwidth. Loss tangent refers to

**Table 1.1.** Common substrates for antenna design.

| Material | Permittivity | Loss Tangent |
|---|---|---|
| Arlon DiClad 870 | 2.33 | 0.0013 |
| Arlon 25FR | 3.58 | 0.0025 |
| FR4 Epoxy | 4.4 | 0.02 |
| Teflon | 5 | 0.03 |
| Alumina 92 pct | 9.2 | 0.008 |

the ratio of imaginary part of permittivity with real part of permittivity. A low loss tangent substrate will increase antenna efficiency and reduces microstrip losses. Thick substrate thickness will maximize bandwidth and efficiency but when it is too thick, surface-wave excitation will occur.

Several patch shapes can be considered in order to obtain a particular radiation pattern, polarization of the fields and input impedance behavior. An important aspect of the design of patch antennas is the feed technique (see Fig. 1.1) [10].

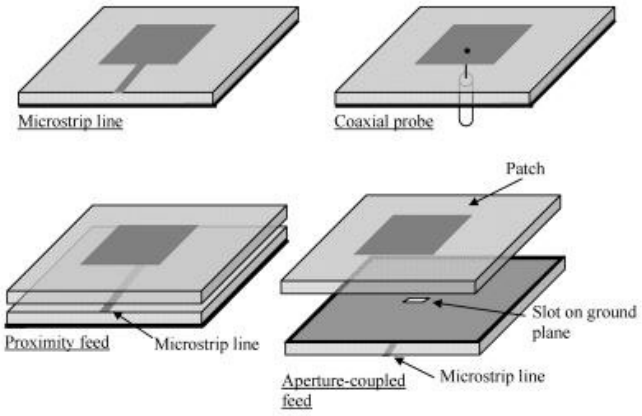


**Fig. 1.1.** Feed techniques for microstrip patch antennas

The simplest feeding method is represented by the use of a microstrip line, terminating with an inset in order to easily tune the value of input impedance.At the edge of a patch, the impedance is generally much higher than 50 ohm (e.g. 200 ohm). To avoid impedance mismatch, sections of quarter-wavelength transformers can be used to transform a large input impedance to a 50 ohm line. With the microstrip-line feed approach, an array of patch elements and their microstrip power division lines can all be designed

and chemically etched on the same substrate with relatively low fabrication cost per element. However, the leakage radiation of the transmission lines may be large enough to raise the sidelobe or cross-polarized levels of the array radiation. Microstrip antennas can also be fed from underneath via a probe. The outer conductor of the coaxial cable is connected to the ground plane, and the center conductor is extended up to the patch antenna. The position of the feed can be altered to control the input impedance.The coaxial probe usually has a characteristic impedance of 50 ohms. Thus the location of the probe should be at a 50 ohm point of the patch to achieve impedance matching. There are a number of terms associated with the coaxial probe. Type N, TNC, or BNC connectors are for VHF, UHF, or lower microwave frequencies. OSM or OSSM connectors can be used throughout the microwave frequencies. OSSM, OS-50 or K-connector are for millimeter-wave frequencies. The coaxial feed introduces an inductance into the feed that may need to be taken into account if the height h gets large, and, in addition, the probe will also radiate, leading to radiation in undesirable directions. In the case of proximity feed the line does not directly touch the antenna. For example, the open end of a 100 ohm line can be placed underneath the patch at its 100 ohm location. An open-ended microstrip line can also be placed in parallel and very close to the edge of a patch, to achieve excitation through fringe-field coupling. Another method of feeding microstrip antennas is the aperture feed. In this technique, the feed line is shielded from the antenna by a common ground plane with an aperture to transmit energy to the antenna. The upper substrate can be made with a lower permittivity to produce loosely bound fringing fields, yielding better radiation. The lower substrate can be independently made with a high value of permittivity for tightly coupled fields that don't produce spurious radiations. The disadvantage of this method is increased difficulty in fabrication, but usually is the method which allows a larger bandwidth. Different definitions of bandwidth have to be taken into account in an antenna design. The first definition is strictly related to the reflection loss at the input terminal, in this case bandwidth is the frequency range over which the input VSWR is less than 2 (or, equivalently,over where the return loss is less than -10dB). A second definition of bandwidth is instead related to the power radiated by the antenna at different frequencies in the main direction. In this case bandwidth is the frequency range in which the radiating power, normalized respect to its maximum, is higher than -3dB. However, this two definitions are strictly related each other. Since the basic configuration allows very narrow fractional bandwidth (usually no more than 5 %) and patch dimensions near to an half wavelength, attempts to achieve compact or wideband microstrip antennas have been widely studied in recent literature for each feeding scheme. The operating bandwidth of a single linearly polarized patch antenna depends by its input reflection loss, which is inversely related to the Q-factor of the patch resonator, and by the quality of radiation. Since Q factor of a patch antenna directly depends on its volume, an effective method to enlarge the bandwidth consists into enlarge the distance between the radiating element

and the ground plane, a very practical solution involves the use of a foam substrate with low permittivity. Usually a coaxial feed is employed and some techniques in order to balance the high inductance of the probe can be considered. As example, in Fig. 1.2, a coaxial fed patch with a thick substrate is shown, with a chip resistor between patch and ground-plane in order to improve input impedance [10].

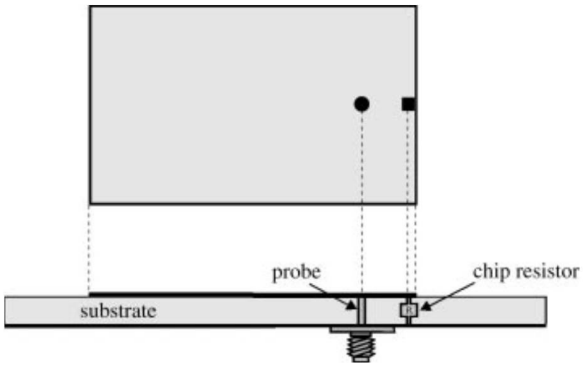


**Fig. 1.2.** Feed compensation through chip resistor for microstrip patch antennas

In Section 1.4 and Chapter 2 of this work, in order to maintain a simple planar design, a capacitive annular slot has been cut in the patch instead of a discrete component to achieve the similar return loss features. As described in Section 1.1, a slot cut into the radiating element introduce additive resonances leading to a wideband behavior. Several slot shapes have been studied in the literature [32, 33], sometimes combined to multi-layer structures based on stacked patches[34]. However in this work a single layer approach has been proposed in order to preserve low profile, and the U-slotted configuration, described in Section 1.3, has been studied as starting point for the proposed innovative design.

## 1.3 U-Slotted Patch Antenna

Slotted patch antennas have been profusely studied in recent literature because of their low profile preserving and easier fabrication respect to stacked configurations, modified feeding schemes, or other techniques of bandwidth enlargement. U-Slotted antennas are probably the most popular of this category, because their are symmetrical and there are few parameters to optimize in order to achieve an acceptable input impedance. The first experimental

study on this typology of antenna was published in 1995, by Huynh and Lee [11] , who developed the basic design provided in Fig. 1.3.

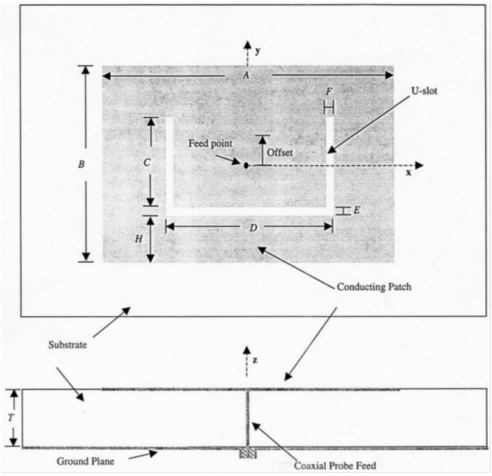


**Fig. 1.3.** Basic U-slot Antenna: front view and lateral view

The feeding point location is chosen to achieve a good input impedance without dramatically waste linear polarization and a foam substrate is inserted between patch and ground-plane in order to further enhance the bandwidth. Even if lots of articles have been written about this topic, few rigorous design procedures and theoretical analysis have been carried out. An equivalent simple circuit has been provided in [35] while a deep analysis, which represent the starting point of the procedure proposed in section 1.4,has been developed in [18], where a qualitative tailoring on the resonant frequencies which cause a wideband behavior are provided. In particular, a first resonant frequency depends on the first slot resonance in the dielectric substrate. Since the input impedance related to this resonance is very high, it does not radiate in a proper way. A second resonant frequency is related to $TM_{01}$ mode of the patch, but since the U-Slot disturbs current path, this frequency is lower than the one performed in the plain patch. A third resonance, due to both x-directed and y-directed modes and mainly related to $TM_{20}$ patch mode, it's a critical aspect of the design, because it can be associated to possible high cross polarization levels within the operative bandwidth of the antenna. The last frequency resonance is mainly the first resonant frequency of the slot in air, moderated by a x-directed resonance of the small pseudo-patch formed inside the U-slot. Approximated formulas relating geometrical parameters of the antenna and these resonant frequency are also provided in [18] and ini-

tial values for the main geometrical parameters of the antenna have been calculated modifying the classic patch antenna design based on transmission line analysis [36]. Patch length may be calculated as follows. The first step is the determination of the effective permeability of the substrate, which can be considered a constant at low frequencies and monotonically increase until its regime value. The initial value is also referred as the static value of the dielectric constant and can be calculated as:

$$\epsilon_{reff} = \frac{\epsilon_r + 1}{2} + \frac{\epsilon_r + 1}{2\sqrt{1 + 12\frac{h}{W}}} \tag{1.1}$$

Once $\epsilon_{reff}$ has been defined, one can calculate the effective length extension due to the fringing effect of the fields at the border of the microstrip.

$$\Delta L = 0.412h\frac{(\epsilon_{reff} + 0.3)(\frac{W}{h} + 0.264)}{(\epsilon_{reff} - 0.258)(\frac{W}{h}) + 0.8} \tag{1.2}$$

Since the length of the patch is effectively incremented in both sides, the effective length can be expressed as

$$L_{eff} = L + 2\Delta L \tag{1.3}$$

So, the length of the patch can be calculated by Eq.1.1 and Eq.1.2 once the substrate height and patch width are known. In particular, patch width, for obtaining a good radiation, can be generally expressed for a microstrip patch antenna as:

$$W = \frac{1}{2f_r\sqrt{\mu_0\epsilon_0}}\sqrt{\frac{2}{\epsilon_{reff} + 1}} \tag{1.4}$$

being $f_r$ the frequency of resonance. In [18], eq 1.4 is considered as a starting value, in fact a back calculation of $L$ is necessary for the design. So:

$$W = 1.5(L + \Delta L) \tag{1.5}$$

and the thickness of the substrate $h$ is chosen as:

$$h = 0.06\frac{\lambda_0}{\sqrt{\epsilon_r}} \tag{1.6}$$

Considering the geometric variables as in Fig. 1.3 and the design proposed in [18], the width of the vertical arms of the slot E,the width F and the length D of the horizontal one can be chosen as:

$$E = F = \frac{\lambda_{res3}}{60} \tag{1.7}$$

$$D = \frac{\lambda_{res2}}{\sqrt{\epsilon_{reff}}} - L + \Delta_L - E \tag{1.8}$$

being $\lambda_{res2}$ and $\lambda_{res2}$ referred to the second and the third resonances described in [18]. Following this design, it is necessary to respect specific constraints for the ratio between the length C and the width D of the slot, in order to force the correct path of currents avoiding x-directed components which cause cross-polarization. In particular:

$$\frac{C}{D} \geq 0.75 \tag{1.9}$$

and between the length of the slot and the width of the patch

$$\frac{C}{W} \geq 0.3 \tag{1.10}$$

For obtaining the distance H between the patch and the horizontal arm of the slot, the effective permittivity and the effective length extension of a pseudo-patch with width

$$W_p = D - 2F \tag{1.11}$$

which corresponds to a patch with the same resonance frequency of the slot. So, replacing Eq. 1.10 into Eq. 1.1 and Eq. 1.12, one obtains

$$\epsilon_{reffPP} = \frac{\epsilon_r + 1}{2} + \frac{\epsilon_r + 1}{2\sqrt{1 + 12\frac{h}{D-2F}}} \tag{1.12}$$

and

$$\Delta L_p = 0.412h\frac{(\epsilon_{reff} + 0.3)(\frac{D-2F}{h} + 0.264)}{(\epsilon_{reff} - 0.258)(\frac{D-2F}{h}) + 0.8} \tag{1.13}$$

So, H can be calculated as:

$$H = L - E + 2\Delta L_p + \frac{1}{\sqrt{\epsilon_{reffPP}}}(\frac{\lambda_{res4}}{4} - 2C - D) \tag{1.14}$$

The value C must be chosen in order to respect the condition

$$L \geq H + E + D \tag{1.15}$$

for achieving a consistent geometry. Even if this study represents an excellent starting point for design, it does not take into account the influence of position of the feed point in both return loss and polarization behavior, and do not solve some drawbacks due to high cross-polar levels caused by horizontal current path if geometry does not respect very strict constraints.

Following the design in [18] is precluded the possibility to design an antenna with reduced size respect to the classic patch.

In order to solve these problems, a new typology of slot is presented in our work, in this case current paths are balanced in order to avoid cross-polarization without complicating the design and in order to achieve a significant compactness respect to both classic patch and U-Slotted patch. In this particular configuration the optimal feeding point is always in the center of the patch and a simple design procedure is proposed in Section 1.4.

## 1.4 Modified U-Slotted Antenna

### 1.4.1 Geometry

As discussed in [18], the combination of antenna and slot modes gives rise to undesired x-directed currents, which produce a high cross-polar field component unless the ratio between the vertical arm C and the horizontal arm D does not satisfy a specific criterion. This means that bandwidth requirements cannot always be satisfied while guaranteeing, at the same time, a low cross-polar effect.The antenna configuration proposed in this work is illustrated in Fig. 1.4. The basic U-slot geometry is properly modified to maintain its bandwidth features, but reducing at the same time the high cross-polar radiation often present at some frequencies within the operating range.

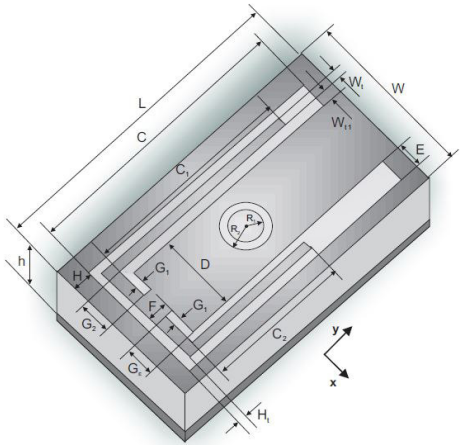


**Fig. 1.4.** Modified U-slot Antenna

As illustrated in Fig.1.4, the U-slot arms are properly shaped to minimize the paths of unwanted x-directed modes. In particular, a cut is realized along the horizontal U-slot direction, thus reducing the extent Ht of the new horizontal arm. To have a better tuning of the operating bandwidth, unequal lengths are chosen for the two U-slot vertical arms, and in order to achieve compactness, current path length has been increased enfolding the vertical arms on themselves. Geometry has been chosen also in order to be suitable for a central feeding point, avoiding the complexity of the effects due to different paths of the current on the slot which cause mismatch and cross-polarization. As a further variation with respect to the existing U-slot design [18], a proper capacitive anular ring is introduced around the feed [36] to compensate for the large probe inductance due to the presence of thick substrates, which could prevent the impedance matching. This problem is particularly evident

at low frequencies, for applications such as P-band radar, where broadband operations impose the use of a large dielectric thickness, with a consequently increased feed inductance strongly limiting the achievable bandwidth to less than 10 %. For comparison purpose, a plot of surface currents distribution of both classic U-Slot Antenna and Modified U-Slot Antenna working at the same central frequency are provided in Fig. 1.5 and 1.6. The simulations have been carried out by Finite Element Method trough the commercial software HFSS 12.

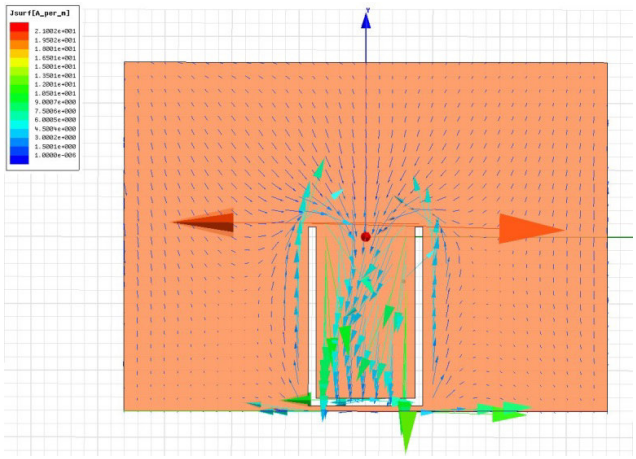

**Fig. 1.5.** Basic U-slot Antenna: Surface currents

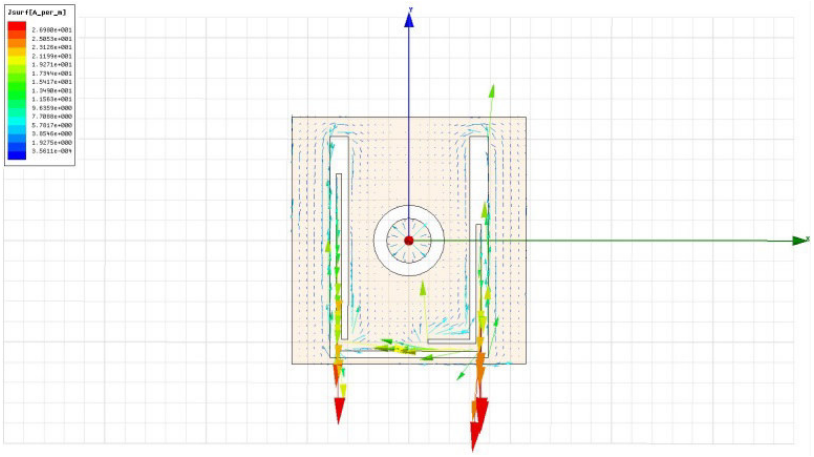

**Fig. 1.6.** Modified U-slot Antenna: Surface currents

In the case of Classic U-Slotted Antenna, a relevant x-directed current circulation can be observed, due to the transition of the current flow around the slot thus causing a more relevant cross-polar level with respect to the configuration proposed in this work where a strong y-directed current component is enforced into the metal stripes inside the vertical arms of the slot. The asymmetrical configuration of the cut permit to balance the flows in order to dramatically decrease the average x-directed current component which causes cross-polarization.

Since the position of resonances is similar in both antennas, simulations in the entire working bandwidth have been performed, achieving the same behavior shown in Fig. 1.5 and Fig. 1.6. Since the scope of the two simulated structure is identical, so one can qualitative note how, achieving the same working frequency range, a dramatic decreasing of patch surface size (about 50 %) is obtained. Once validate the effectiveness of the design, a campaign of extensive simulations have been carried out through Method of Moments analysis in order to find a model, similar to the one proposed in [18] , which quantitative describes an effective design technique for the Modified U-Slot Antenna.

### 1.4.2 Empirical model for design

While the behavior of the resonant frequency is similar in both classical and modified U-Slot Antennas, an improved design strategy has been developed in this work to face the problems due to the frequency shift and high cross-polar radiation, both caused by the hybrid combination of the patch and the slot modes, without introducing particular constraints in the design once calculating the geometrical parameters. Starting from the studies in [18] , cited in Section 1.3, a simple empirical method, based on the adaptation of the existing formulas for microstrip patch antenna and microstrip U-Slotted patch antenna to the proposed design, has been proposed. At this purpose, the antenna layout is properly modified as described in Subsection 1.4.1, with the further inclusion of a proper anular ring to guarantee the prescribed wideband features even in the presence of thick substrates, usually required at low frequencies for an effective Q factor lowering and a significant bandwidth improvement. The details of the proposed design procedure are described by the following steps:

- Fixed the design central frequency $f$, compute the shifted frequency $f_0$ to be adopted in the successive parameters evaluation, by the expressions:

$$f_0 = 1.101f - 0.043[GHz], f \leq 2.75GHz \tag{1.16}$$

$$f_0 = 1.214f - 0.3539[GHz], 2.75GHz \leq f \geq 4.975GHz \tag{1.17}$$

$$f_0 = 1.101f - 0.043[GHz], 4.975GHz \leq f \geq 10.1GHz \tag{1.18}$$

- From the knowledge of the shifted frequency, compute the value of the patch width W by the expression:

$$W = \frac{c}{3.55 f_0}\sqrt{\epsilon_{reff}} \tag{1.19}$$

and the value of the patch length L solving equation 1.3 , but using, for substrate thickness, the equation:

$$h = \frac{c}{11 f_0} \tag{1.20}$$

From the equations reported above, a significant reduction of the overall antenna dimension (up to 40 %) is obtained with respect to the designs existing in literature [18]. Furthermore, the new expression provided for the substrate thickness automatically satisfies the rule imposed in [18], fixing a lower limit below which a broadband operation is not obtainable. On the basis of the proposed empirical formulas, it is straightforward to derive that, in the presence of low permittivity substrates, the values of patch dimensions W and L are quite similar and the patch is almost square.

- Compute the geometrical parameters $E$ , $F$, $H_T$ , $G$ , $W_T$ , $W_{T1}$, $G_1$ and H by the following expressions:

$$E = F = \frac{c}{35 f_0} \tag{1.21}$$

$$G_\epsilon = G + G_\delta \tag{1.22}$$

$$G = \frac{0.0888c}{f_0} \tag{1.23}$$

$$G_\delta = 0.0157\frac{c}{f_0}(\sqrt{\epsilon_r} - 1) \tag{1.24}$$

$$Wt = \frac{E}{3} \tag{1.25}$$

$$W_{t1} = H = G_1 = H_t \tag{1.26}$$

Compute the U-slot width D according to the existing model [18], but adopting the new geometrical parameters as:

$$D = \frac{c}{\alpha f_0 \sqrt{\epsilon_r}} - 2(L + 2\Delta_L - E) \tag{1.27}$$

where the term $\alpha$ is the only tuning parameter adopted in the synthesis procedure, whose values can be chosen in the range between 0.8 and 0.92 to guarantee an adequate matching in the operating frequency range.

- Compute the total U-slot vertical length C by the new expression:

$$C = L - \Delta_L \tag{1.28}$$

and the parameters C1 and C2 of the Modified U-Slot by the following expressions:

$$C_1 = (\frac{c}{4f_0\sqrt{\epsilon_r}} - \frac{E}{2})(1 + \frac{D\alpha f_0}{c}) \tag{1.29}$$

$$C_2 = (\frac{c}{4f_0\sqrt{\epsilon_r}} - \frac{E}{2})(1 - \frac{Df_0}{\alpha c}) \tag{1.30}$$

- Compute the values of the inner and outer radii $R_1$ and $R_2$ as follows:

$$R_1 = 6.189 * 10^6 {f_0}^{-0.9535}[m] \tag{1.31}$$

$$R_2 = 2.577 * 10^5 {f_0}^{-0.8166}[m] \tag{1.32}$$

with $f_0$ in Hz.

The outlined method for the synthesis of Modified U-Slotted Antenna highlights a significant difference with respect to the design procedure proposed in [18]. As a matter of fact, in the original approach, the operating bandwidth is always fixed equal to the difference between the fourth and the second resonant frequencies of the structure. This criterion does not always guarantee to achieve the desired frequency band operation, and the useful antenna bandwidth could be less than the fixed one, as declared by the same authors in [18]. In our approach, the modified U-slot configuration, together with the adopted circular ring, leads to have a minimum useful bandwidth of 15 %, which can be simply obtained by applying the synthesis procedure outlined into this section. A few iterations with respect to the parameter $\alpha$ are required to optimize the matching in the operating frequency range and the overall design procedure is able to guarantee a frequency band between 15 % and 20 %. The empirical formulas presented in the previous section are numerically validated at different operating frequencies between 1 GHz and 10 GHz. Firstly, three prototypes are designed, respectively working at 1.8 GHz, 3.5 GHz and 7 GHz, by assuming a foam substrate ( $\epsilon_r = 1.07$). The synthesis procedure is applied for all assumed designs, starting from a value of $\alpha = 0.88$ and using a step $\Delta\alpha = 0.01$ . The process is stopped after a few iterations (typically between 2 and 4), when reaching a bandwidth of about 15 %. All designed antennas have a thickness h as given by 1.20. In 1.2, 1.3 and 1.4 the value of all geometrical parameters , according to the proposed model, are presented for each frequency.

The return loss curves for the three prototypes, reported in Fig. 1.7, Fig. 1.8, and Fig. 1.9, properly show a bandwidth of about 15 %, as imposed in the synthesis procedure.

**Table 1.2.** Modified U-Slot Antenna dimensions @ 1.8 GHz and $\alpha = 0.92$

| Parameter | Dimension [mm] | Parameter | Dimension [mm] |
|---|---|---|---|
| L | 58.1 | D | 21.9 |
| W | 53.3 | E | 4.4 |
| C | 49.4 | F | 4.4 |
| $C_1$ | 39.8 | $W_t$ | 1.5 |
| $C_2$ | 29.8 | G | 11.9 |
| $H_t$ | 1.5 | $R_2$ | 8.6 |
| H | 1.4 | $R_1$ | 6.7 |
| $G1$ | 1.5 | $W_{t1}$ | 1.5 |

**Table 1.3.** Modified U-Slot Antenna dimensions @ 3.5 GHz and $\alpha = 0.91$

| Parameter | Dimension [mm] | Parameter | Dimension [mm] |
|---|---|---|---|
| L | 28.9 | D | 11.8 |
| W | 26.5 | E | 11.2 |
| C | 24.5 | F | 2.2 |
| $C_1$ | 20.0 | $W_t$ | 0.7 |
| $C_2$ | 14.6 | G | 6.3 |
| $H_t$ | 0.7 | $R_2$ | 4.1 |
| H | 0.7 | $R_1$ | 3.6 |
| $G1$ | 0.7 | $W_{t1}$ | 0.7 |

**Table 1.4.** Modified U-Slot Antenna dimensions @ 7 GHz and $\alpha = 0.90$

| Parameter | Dimension [mm] | Parameter | Dimension [mm] |
|---|---|---|---|
| L | 13.76 | D | 6.07 |
| W | 12.65 | E | 1.05 |
| C | 11.7 | F | 1.05 |
| $C_1$ | 9.58 | $W_t$ | 0.35 |
| $C_2$ | 6.81 | G | 3.05 |
| $H_t$ | 0.35 | $R_2$ | 2.18 |
| H | 0.34 | $R_1$ | 2.07 |
| $G1$ | 0.34 | $W_{t1}$ | 0.34 |

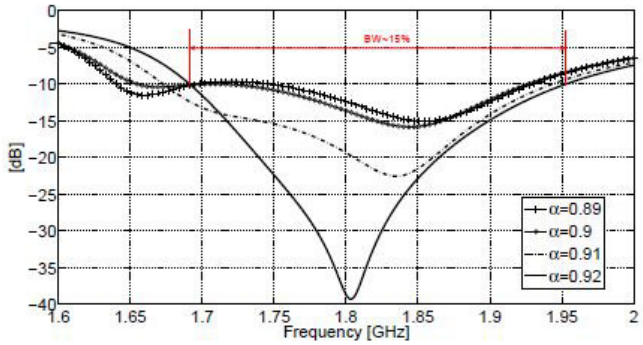


**Fig. 1.7.** Simulated return loss of MUSA @ 1.8 GHz

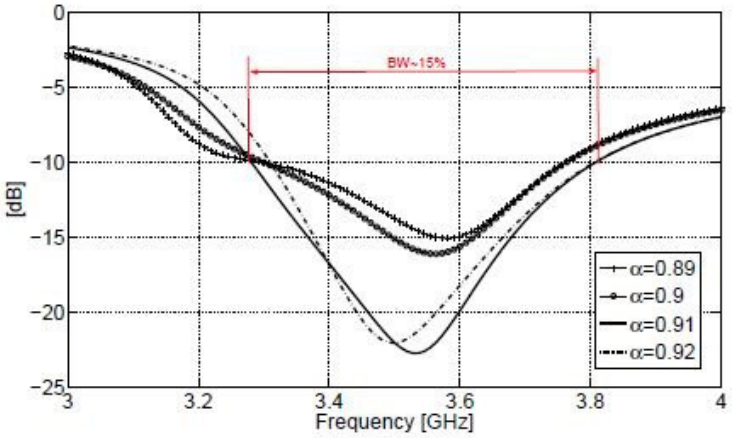


**Fig. 1.8.** Simulated return loss of MUSA @ 3.5 GHz

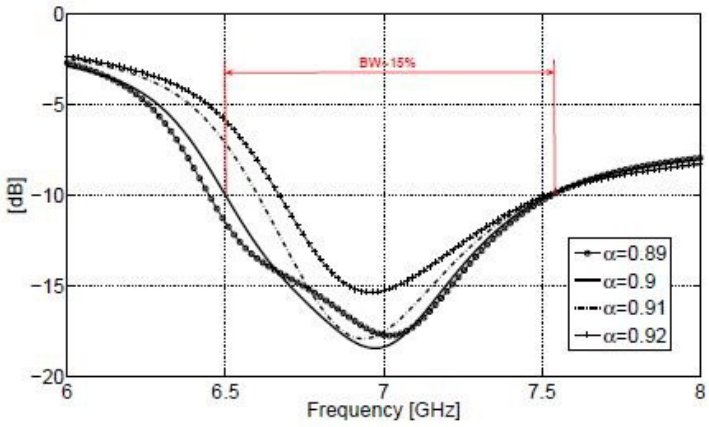


**Fig. 1.9.** Simulated return loss of MUSA @ 7 GHz

A plot of far fields, for each frequency range design, is provided in Fig. 1.10, Fig. 1.11, and Fig. 1.12

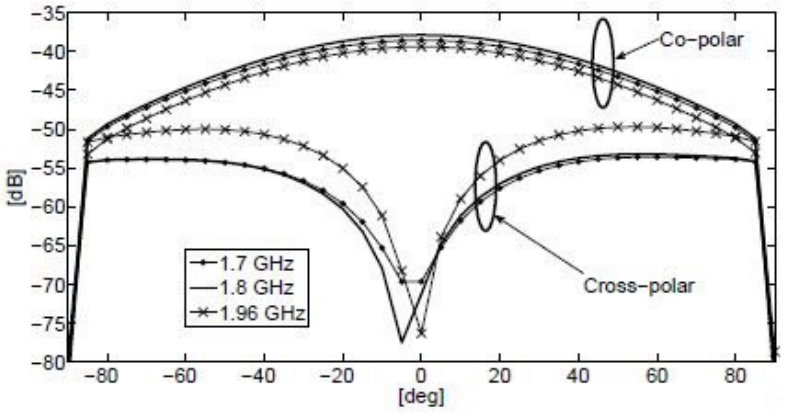


**Fig. 1.10.** Simulated radiation pattern @ 1.8 GHz

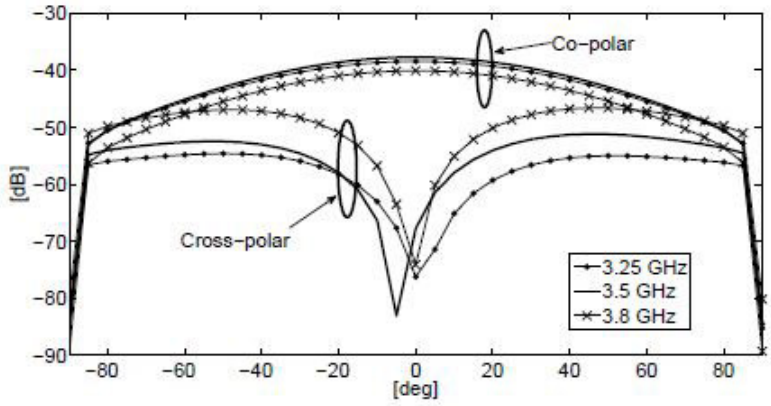


**Fig. 1.11.** Simulated radiation pattern @ 3.5 GHz

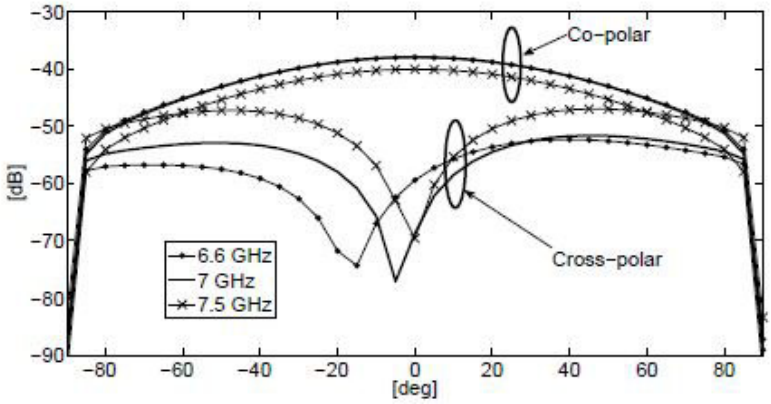


**Fig. 1.12.** Simulated radiation pattern @ 7 GHz

Far-field patterns (H-plane), indicate a cross-polar level, at the central operating frequency, properly below the co-polar one, with a difference of about 33 dB between them along the main beam direction. This good cross-polar behavior is maintained within the full frequency range, as it can be observed in the same figures at different operating frequencies. Similar behavior have been obtained in the E-Plane.

## 1.5 Experimental results

### 1.5.1 P-Band Prototype

In order to assess by experimental results the validity of the proposed synthesis procedure on Modified U-Slot Antenna, two different prototypes suitable for P-band and C band radar applications have been realized and successfully tested in the Microwave Lab at University of Calabria. A first prototype is assumed to work at a central frequency $f_0 = 450MHz$, with an operating bandwidth of about 15 %, useful for P-sounding radar. A foam substrate ($\epsilon_r = 1.07$) is assumed, with an upper thin layer (0.762 mm) of dielectric Diclad870 ($\epsilon_r = 2.33$), uniquely adopted for robustness reason, to better support the U-shaped slot. Design rules presented in [18] are considered to have a starting (and reference) point for developing two different classic U-slot antennas, the first one without optimization respect to the model proposed in [18] (Design 1) and the second one after an optimization of both bandwidth and dimensions (Design 2), as reported in Tab. 1.5; these designs are produced in order to directly compare the performance of the existing U-Slot Antenna with the prototype proposed in this study.

**Table 1.5.** Designed Classic U-Slot Antennas main dimensions

| Configuration name | Patch Width [W] | Patch Length [mm] |
|---|---|---|
| Design 1 | 49.26 | 27.50 |
| Design 2 | 36.10 | 26.12 |

In Fig. 1.13 is shown the return loss of both configurations.

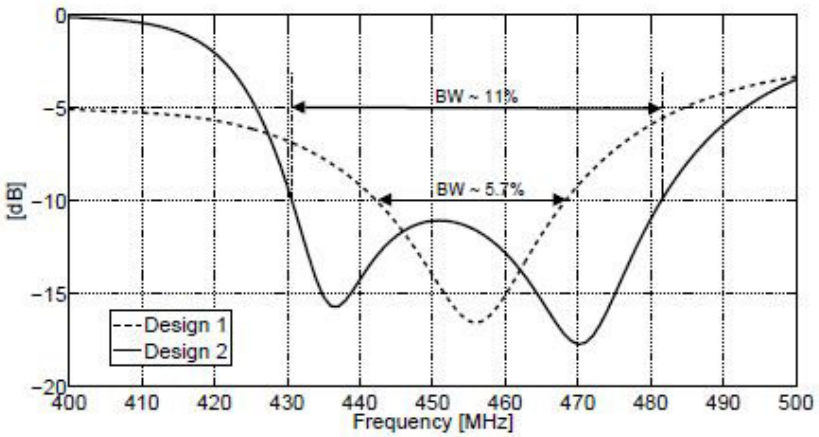


**Fig. 1.13.** Simulated Return Loss performed by designed Classic U-Slot Antennas

Simulated return loss (Fig.8) shows a reduced bandwidth of about 5.7 % with respect to the imposed constraint, thus requiring an optimization refinement to obtain Design 2 configuration also reported in 1.5. A larger bandwdith of about 11% is obtained in this case, but lower again with respect to the prescribed goal of 15 %. Furthermore, when approaching the frequency band extremes, a cross-polar field level in the H-plane comparable to the co-polar component is produced, as yet observed in [18], thus indicating a reduction of the effective useful bandwidth, as shown in Fig. 1.14, where both co-polar and cross-polar field components of Design 2 configuration, are shown at different frequencies belonging to the operative Return Loss bandwidth of the antenna.

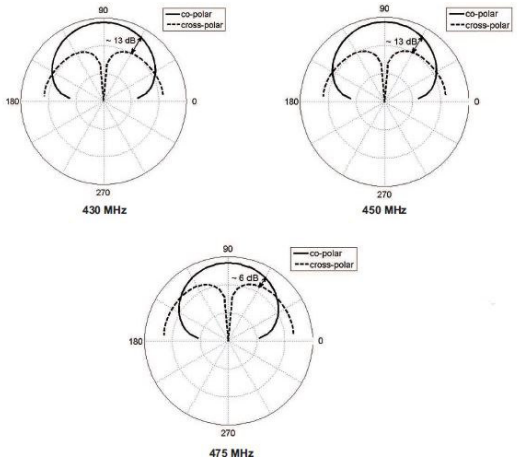


**Fig. 1.14.** Simulated Radiation Pattern performed by designed optimized Classic U-Slot Antenna

To overcome cross-polar limitations of Standard U-Slot Antenna design, the modified structure presented in 1.4.1 has been developed using the procedure described in 1.4.2, without further optimization steps. The values assumed by the geometrical parameters, obtained through the empirical model proposed, are indicated in 1.6, while a photograph of the fabricated prototype, during a far field measurement in the anechoic chamber at University of Calabria, is shown in Fig. 1.15.

**Table 1.6.** Modified U-Slot Antenna: dimensions of P-Band Prototype

| Parameter | Dimension [cm] | Parameter | Dimension [cm] |
|---|---|---|---|
| L | 24.3 | D | 15.6 |
| W | 23.1 | E | 1.8 |
| C | 21.8 | F | 1.8 |
| $C_1$ | 18.1 | $W_t$ | 0.5 |
| $C_2$ | 23.1 | G | 5.9 |
| $H_t$ | 0.5 | $R_2$ | 3.5 |
| H | 0.6 | $R_1$ | 2.2 |
| $G1$ | 0.5 | $W_{t1}$ | 0.5 |

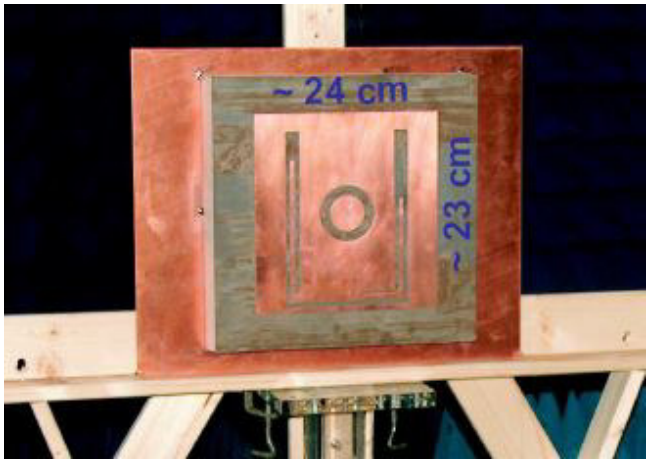


**Fig. 1.15.** Photograph of P-Band Prototype during a far field measurement

The P-band antenna is tested into the Microwave Laboratory at University of Calabria, in terms of return loss response as well as radiation pattern behavior. A bandwidth of about 15 % is successfully obtained, with a very good agreement between simulated (Ansoft Designer Version 3.5) and measured data, as reported in 1.16.

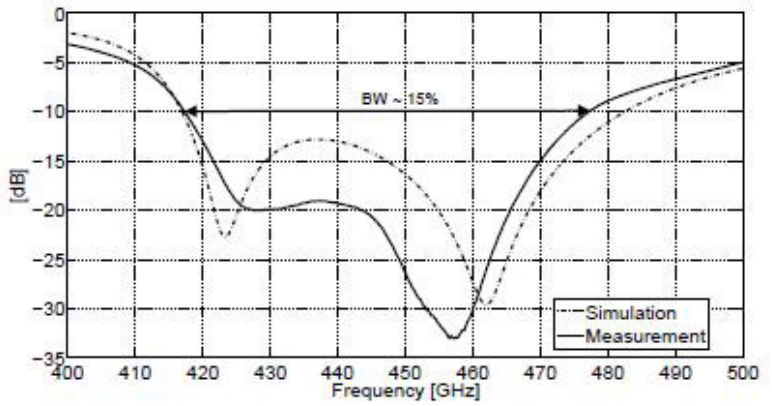


**Fig. 1.16.** Simulated and measured return loss of P-Band Modified U-Slot Antenna Prototype

Furthermore, the wideband response is confirmed by the radiation features, illustrated in 1.17, for both H-Plane and E-Plane.

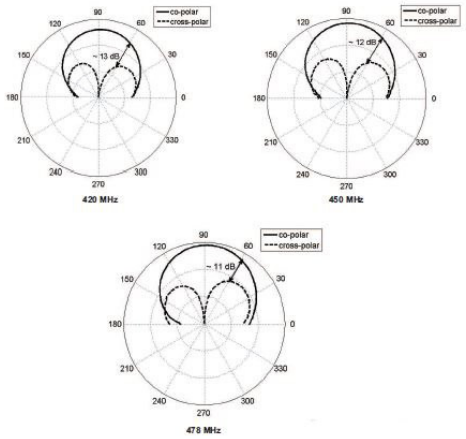


**Fig. 1.17.** Simulated and measured return loss of P-Band Modified U-Slot Antenna Prototype

The cross-polar component remains properly below the co-polar field at the frequency band extremes, while in the original reference design [65] a poor difference of about 6dB between the co-polar and cross-polar ones is performed in the upper bound frequency limit. As a further improved feature with respect to Standard U-Slot Antenna, is the strong size reduction of the prototype, equal to 50 % of the total area surface. In order to provide a final verification of the wideband behavior of the fabricated prototype, a multi-frequency radiation pattern measurement has been performed in the anechoic chamber, the measured gain in the azimuth plane vs frequency is shown in Fig. 1.18

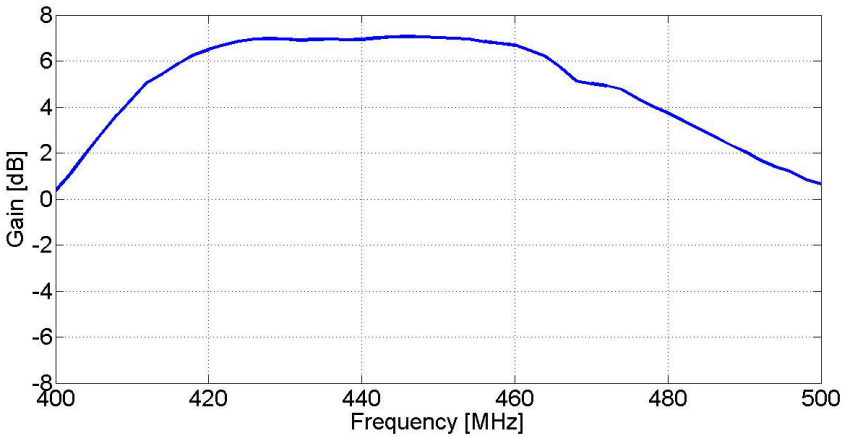


**Fig. 1.18.** Measured gain vs frequency of P-Band Modified U-Slot Antenna Prototype

A wideband -3dB frequency range has been performed, thus confirming the wideband feature of the measured return loss.

### 1.5.2 C-Band Prototype

In order to further experimentally validate the empirical model, the same design process to that adopted for the P-band prototype is applied to synthesize a C-band antenna, working at a central operating frequency $f_o = 4.3$ GHz. A foam substrate ( $\epsilon_r = 1.07$) is again assumed, with an upper thin (0.762 mm) layer of standard dielectric Di-Clad 870 ( $\epsilon_r = 2.33$) to mechanically enforce the radiating structure, as in the previous case. The synthesis procedure outlined in Section 3 is applied by initially assuming a value $\alpha = 0.89$ , and obtaining, after a few iteration steps ( $\alpha = 0.91$), the final configuration whose dimensions are reported in 1.7.

The correct behavior of C-Band prototype (Fig. 1.19 ) is firstly tested by measuring the return loss, which is successfully compared in Fig. 1.14 with the simulation results (performed with Ansoft Designer v 3.5).

**Table 1.7.** Modified U-Slot Antenna: dimensions of C-Band Prototype

| Parameter | Dimension [mm] | Parameter | Dimension [mm] |
|---|---|---|---|
| L | 25.1 | D | 11.0 |
| W | 19.4 | E | 1.9 |
| C | 21.5 | F | 1.9 |
| $C_1$ | 18.1 | $W_t$ | 0.6 |
| $C_2$ | 13.0 | G | 5.5 |
| $H_t$ | 0.6 | $R_2$ | 3.9 |
| H | 0.6 | $R_1$ | 3.4 |
| $G1$ | 0.5 | $W_{t1}$ | 0.5 |

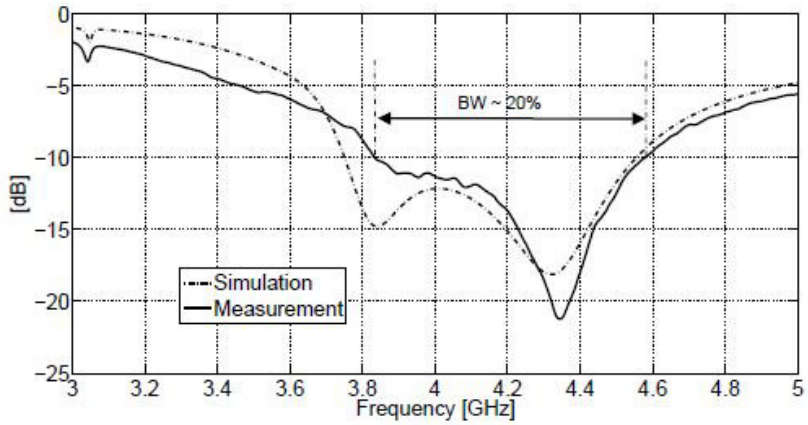


**Fig. 1.19.** C-Band prototype: comparison between simulated and measured return loss

In this case the fabricated antenna shows a large measured bandwidth approximately equal to 20 %. The wideband feature is further confirmed by the measured radiation patterns in Fig. 1.20 .

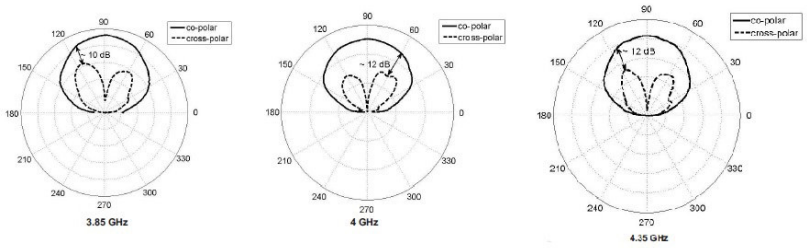


**Fig. 1.20.** C-Band Prototype: far field measurements

Cross-polar components properly remain at an acceptable level below the co-polar field within the operating frequency range, like with P-Band Prototype. Also in this case, a compact antenna (about half-size in respect to the standard configuration) with broadband features and reduced cross-polar effects is obtained. In order to further validate the wideband behavior of the proposed antenna, radiation patterns have been tested at different frequencies in -10dB frequency range. A plot of measured gain vs frequency in H-Plane is shown in 1.21, while identical results have been performed in E-Plane measurements.

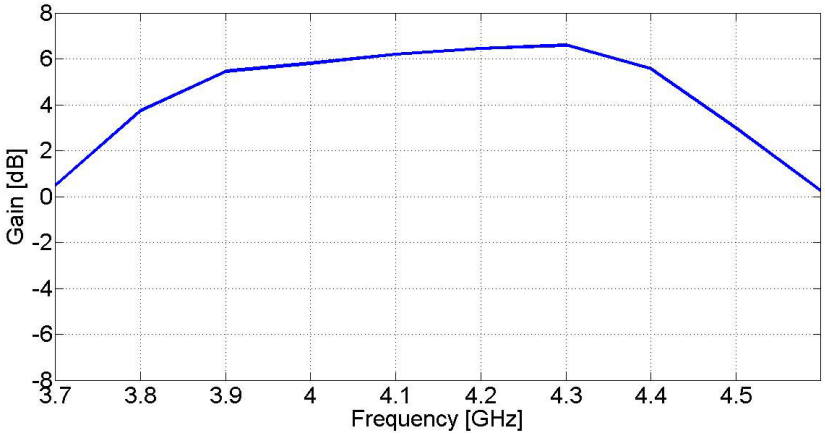


**Fig. 1.21.** Measured gain vs frequency of C-Band Modified U-Slot Antenna Prototype

Wideband behavior is confirmed by gain measurement, with a peak value around 7dB, similar to classic microstrip antenna configurations, according to a -3dB gain bandwidth even larger than the -10dB return loss one. So, the

new geometry layout for compact U-slotted patch proposed in this chapter, with improved features in terms of cross-polarization effects, may represent a valid antenna design in those radar applications which require a broadband behavior without wasting its performance in terms of quality of the radiation pattern but maintaining reduced surface area and an easy fabrication process. Arrays made up by a simplified version of the proposed antenna have been integrated in two different innovative radar system. The design of the antenna, the experimental validation of the simplified design and a brief discussion on the feature of the whole radar systems, are provided in Chapter 2 of this work.

# 2

# Ring Slotted Patch Antenna for radar applications

## 2.1 Ring Slotted Patch Antenna: Generalities

A correct design of antennas is a critical aspect for a generic radar system, especially for modern devices which allow the possibility to switch different operative modes. Software Defined Radar Systems and Multi-Mode Multi-Frequency Radars (briefly described in this chapter) allow a huge flexibility in respect to the previous devices, permitting to change some operative parameters on fly in order to practically modify their functions in the strength of the scenario their are operating. Clearly, a reuse of hardware components for different purposes (Multi-Mode Radar) or the substitution of hardware components with software modules which perform the same function also permit a consistent advantage in terms of costs. As described in Subsection 2.2 and Subsection 2.3 , in order to maintain these features, avoiding performance bottlenecks and cost increasing, the radar antenna have to be designed respecting several constraints, usually stronger than the one for other applications.

Since different polarization of the scattered waves give different information in the scenario under analysis, a particular attention have to be paid to the cross-polar level, especially if the radar is designed to operate with a linear polarization and the signal process modules need a very clean received signal to obtain significant results . Bandwidth is another critical aspect, especially for Software Defined Systems, in fact a broadband antenna does not reduce the flexibility of the radar system if new signal processing algorithms are gradually added after final hardware design. A large bandwidth is also necessary to achieve the high resolution required by most of modern applications. Compactness and low profile are also required if the operating frequency is relatively low (as P-Band applications) or an array of lots of elements is needed in order to have a sufficient narrow beam width. Small differences in weight and size of antennas, for some specific scenarios (like aerospace applications), may lead to a huge increment of implementation and management costs, so a good trade-off between electromagnetic properties and geometric properties of transmitting and receiving antennas, are necessary for their suitability in

the radar field. In this section, a simplified version of the Modified U-Slotted Antenna proposed in Chapter 1, has been integrated in two different radar systems. The basic layout is shown in Fig. 2.1

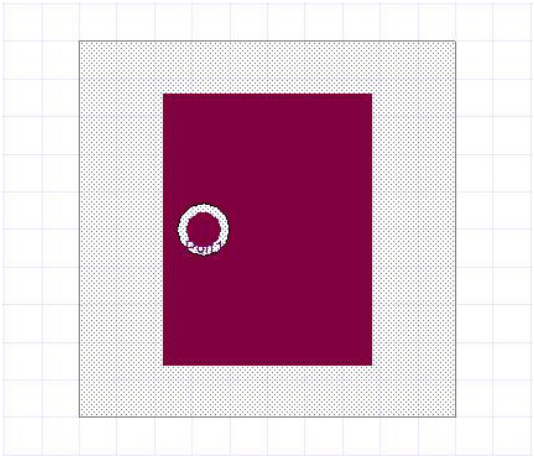

**Fig. 2.1.** Single-Polarization Ring Slotted Antenna: Top Layer Layout

Basic equation for Microstrip Rectangular Patch length (Eq. 1.3) and the proposed one for Modified U-Slot Antenna patch width (Eq. 1.19) have been used as a starting point for the design. A starting point for finding the geometrical parameters of the ring are provided, like proposed in Chapter 1 for the complete configuration, in Eq. 1.31 for the outer radius and Eq. 1.32 for the inner one. Even if in this case an optimization of the geometric parameter is required, achieving a good trade-off between large bandwidth behavior and compactness of the surface area is possible after few tuning of the main geometrical variables.

Even if the first theoretical analysis of the ring shaped slot around the feeding point has been developed in [37], the structure proposed in this chapter is, by our knowledge, the first one allowing a dual-polarization design. In particular, the layout outlined in Fig. 2.1 has been properly modified to simultaneously allow both vertical and horizontal polarization, as shown in Fig. 2.2.

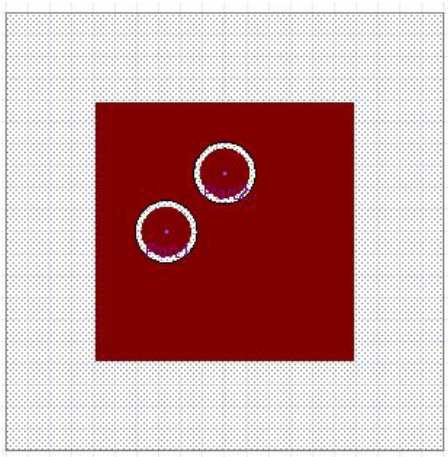

**Fig. 2.2.** Dual-Polarization Ring Slotted Antenna: Top Layer Layout

Starting from the design of a single polarized antenna, with the duplication of the feeding and the annular slot, after few variations of the geometrical parameters a large bandwidth can be obtained, according to a significant size reduction and an acceptable isolation between the two polarization, quite improved by the circular ring. This simple design represent the basic element for design of the antenna arrays integrated into the two radar system described in Section 2.2 and Section 2.3.

## 2.2 Ring Loaded Patch Array for Landslides Early Warning Radar Design

### 2.2.1 System Description

Military operation, like target detection, target recognition, surveillance, and other specific applications, like meteorology and air-traffic control, had represented, in the early development of radar technology, the main field of application. However, in the same way as other electronic devices, in the recent years a large amount of new possible applications, in different disciplines (automotive, medical science, biology), have been outlined. In order to satisfy requirements due to large-scale commercial applications, modern radar systems have to perform the same operations typical of a classical radar, but according to significant cost reduction and a strong adaptability. A new concept of design, called Software Defined Radar (SDRadar), may lead to new interesting developments in radar technology because of the possibility of performing most of the basic operations (i.e., mixing, filtering, modulation and demodulation) employing software modules in order to eliminate most of the specific hardware and their costs [38].

Since signal generation and signal processing parameters may be easily adapted on the fly to the task under consideration, another important advantage due to the Software Defined approach is related to a significant improvement in the versatility of the system. The solution proposed by the team of Microwave Lab at University of Calabria, for a low cost SDRadar system development, has been obtained by the adoption of the Universal Software Radio Peripheral (USRP) transceiver. A first attempt to apply USRP for target detection was performed in [39], in which a SDRadar system was implemented through the use of first generation USRP, but the narrow bandwidth imposed by the available USB connection limited the resolution. So, USRP NI2920, which allows a larger bandwidth respect to the USRP of first generation, has been considered for developing a Software Defined Radar [40]. The design proposed in [39] has been developed to create a low cost, compact and flexible solution; potentially this scheme can be easily employed in different use cases without significant hardware modification, with the possibility to create a multi-purpose radar system. A simplified block diagram of the SDRadar system is reported in Fig. 2.3.

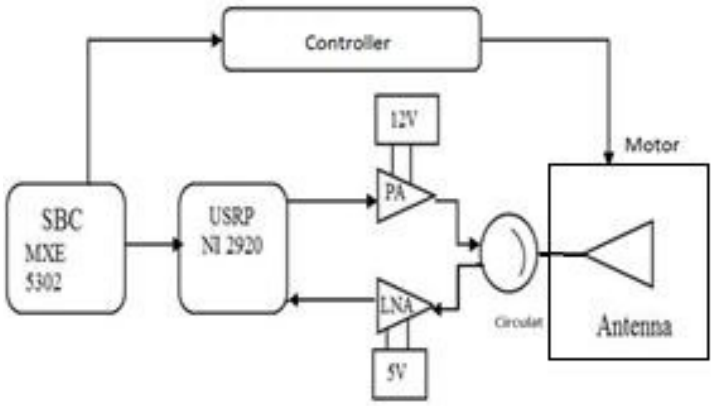


**Fig. 2.3.** Software Defined Radar System: block diagram

The USRP 2920 platform is used to transmit and receive data by a linear array antenna composed by the element proposed in this chapter. The whole system is controlled by a LabVIEW application running on a compact Single Board Computer (SBC). It is able to perform the signal processing useful for the characterization of the area under analysis, but it is designed also to control a motor system permitting to rotate the antenna, thus giving a scanning feature useful for an accurate surface monitoring in different directions. A Power Amplifier (PA) and a Low Noise Amplifier (LNA) increase the signal power along both the transmission and the receiving paths and a

circulator has been used in the indoor test to employ a unique antenna both in transmission and in receiving path, further reducing the total hardware costs and the size of the entire device. In particular, by signal processing point of view, a Stretch Processing approach has been implemented in the system to fully take advantage of the benefit of NI2920 enhanced bandwidth. In order to penetrate vegetation, L-Band frequency range as been chosen, according to an horizontal polarization of antennas.

In outdoor tests, however, two distinct antennas have been adopted in transmission and receiving path in order to improve Signal to Noise Ratio. The final prototype has been successfully integrated in the project $PON01-01503$, financed by European Community , in which several Italian teams have collaborated, most of them belonging to University of Calabria. The main aim of the project is related to the landslide Early warning on Italian highways.

### 2.2.2 Antenna Design and Experimental Results

Starting by the design method developed in Chapter 1 of this work, but applied to the simplified version proposed in 2.1, an array of antennas has been synthesized, fabricated and tested in order to be easily integrated in the software defined radar for landslides early warning application briefly described in the first part of this section. So, according to layout in Fig. 2.1, a large band ring slotted patch antenna, with horizontal polarization has been developed, and the dimensions of main geometrical parameters on the basic cell are provided in Tab. 2.1. Dimensions are related to a L-Band prototype, working at the central frequency of 1.8 GHz, according to the radar operative frequency. Starting by dimensions outlined in Tab. 2.1, an array composed by 8x4 elements has been designed in order to completely satisfy the constraints due to

**Table 2.1.** Geometrical parameters of horizontal polarized ring slotted antenna

| Parameter | Value [mm] |
|---|---|
| Ground Plane Length | 100 |
| Ground Plane Width | 100 |
| Patch Length | 72 |
| Patch Width | 55 |
| External Ring Radius | 7 |
| External Ring Radius | 4.55 |
| Feed Point Coordinates | ( -17, 0) |
| Foam Height | 20 |
| Support Substrate Height | 0.762 |

the integration with the rest of the radar system. In particular, the top layer of the entire array is provided in Fig. 2.4 .

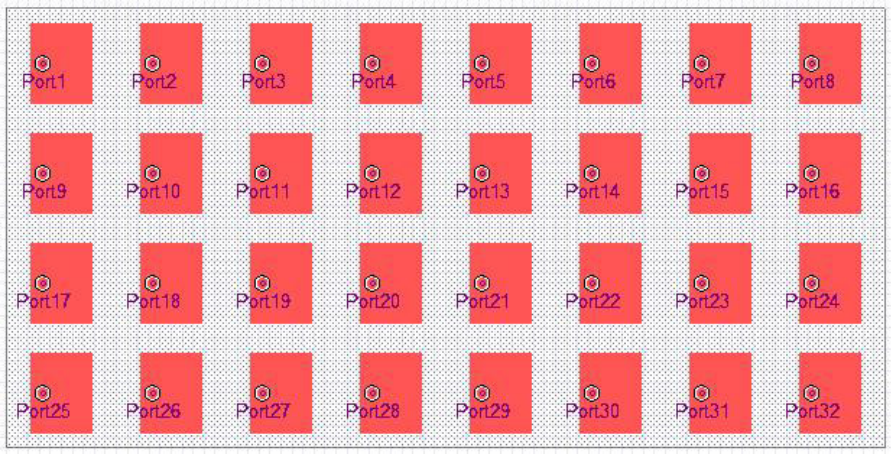


**Fig. 2.4.** Top layer of L-Band Ring Loaded Microstrip Patch Array

Total dimensions of the array are 80x40 cm, while the distance between contiguous elements is 10cm, equal to 0.6 wavelengths at the central frequency 1.8GHz. Simulations were carried out with both Method of Moments (using the commercial software Ansoft Designer V. 3.5) and Finite Element Method (using Ansoft Hfss V. 12), but results were substantially the same. A plot of the return loss at port 1 (referred to the design in Fig. 2.4 ), produced by using MoM, is provided in Fig. 2.5.

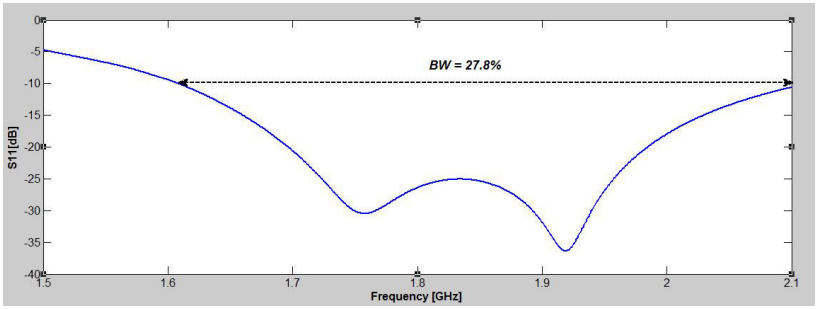


**Fig. 2.5.** Simulated Return Loss for port 1 of L-Band Ring Slotted Patch Array

As in the case of Modified U-Slotted Antenna outlined in Chapter 1 of this work, wideband operations are achieved (27.8 % respect to the central

frequency), according to a significant size reduction of the radiating element. Clearly, dimensions of the single radiating elements does not affect significantly total dimensions of the array (since the total number of elements in a column or in a row is established in order to obtain a certain beam width in the elevation plane or in azimuth plane), however, a small size element dramatically reduce coupling between contiguous elements when the distance between them is fixed a priori. So, in Fig. 2.6 is shown the transmission coefficient between Port 1 and the contiguous ports.

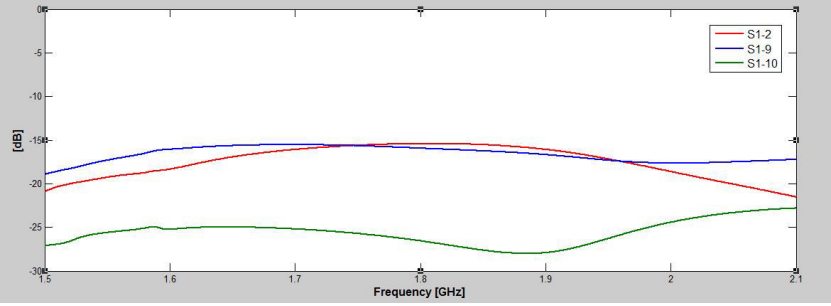


**Fig. 2.6.** Simulated S parameters from port 1 to the contiguous ports of L-Band Ring Slotted Patch Array

One can notice how the simulated transmission coefficients between contiguous port remain under the threshold of -15dB, maintaining a flat behavior, in the entire operation bandwidth. How explained in Chapter 1, a fundamental aspect of a radar antenna design deals with the maintaining of a low cross-polar level in both E-Plane and H-Plane, especially in the angle range effectively scanned by the radar system, in the entire frequency range. In Fig. 2.7 is shown the simulated radiation pattern, in both E-Plane and H-Plane, at the central operating frequency of 1.8GHz.

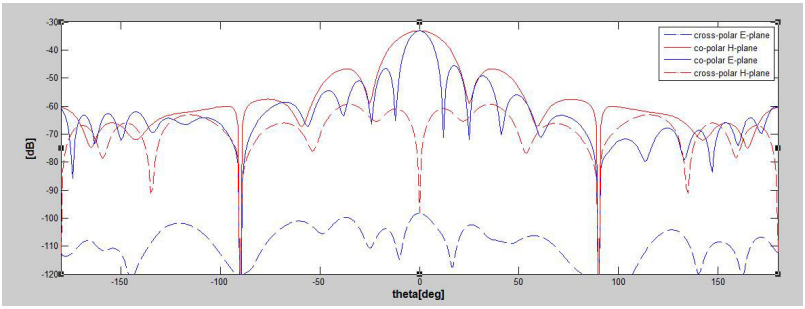


**Fig. 2.7.** Simulated Radiation Pattern @ 1.8 GHz

How shown in 2.7, proposed array achieves a beam width of 10 degrees in the azimuth plane and 21 degrees in the elevation plane, how required by the application. Cross-polar electric field components are properly below the co-polar one for both E-Plane and H-Plane in the whole useful scanning angle range, especially in broadside direction, radiation pattern maintains its symmetry neitherless the presence of the annular slot with contributes to radiation. Peak gain is about 21 dBi. In order to further validate results obtained by this design, radiation pattern has been simulated in the lower extreme of -10dB Return Loss bandwidth (Fig. 2.8) and in the upper one (Fig. 2.9).

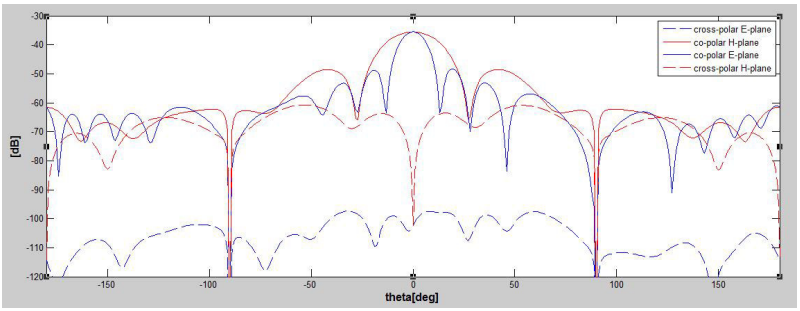


**Fig. 2.8.** Simulated Radiation Pattern @ 1.6 GHz

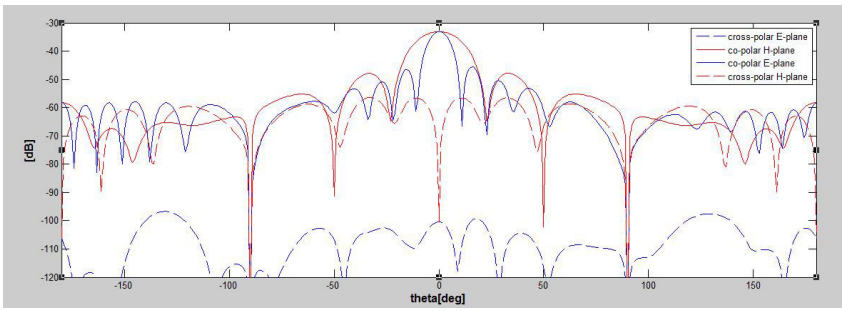


**Fig. 2.9.** Simulated Radiation Pattern @ 2.0 GHz

Cross-polar level of field components is properly maintained below the co-polar level, no significant variations between radiation patterns at the different frequencies in the operative bandwidth can be appreciate neither in the radiation shape nor in the peak value, so a -3dB radiation pattern bandwidth larger than the return loss bandwidth has been achieved. The designed prototype has been fabricated in the Microwave Lab of University of Calabria.

For practicability, two identical square modules of 4x4 elements have been realized and placed side by side. The two realized modules have been realized through an LPKF numerical control machine while coaxial feed have been manually soldered to the ground-plane and further connected to the plane containing the radiating elements, by piercing the foam block. Different blocks have been assembled using a thin adhesive substrate of Arlon CuClad 870, with the same permittivity of the support substrate (Arlon DiClad 870) in order to avoid to introduce useless discontinuity in the structure. An additive substrate composed by fiberglass has been inserted under the ground-plane for increasing the robustness of the structure. In Fig. 2.10 is provided a photograph of a module, before assembly.

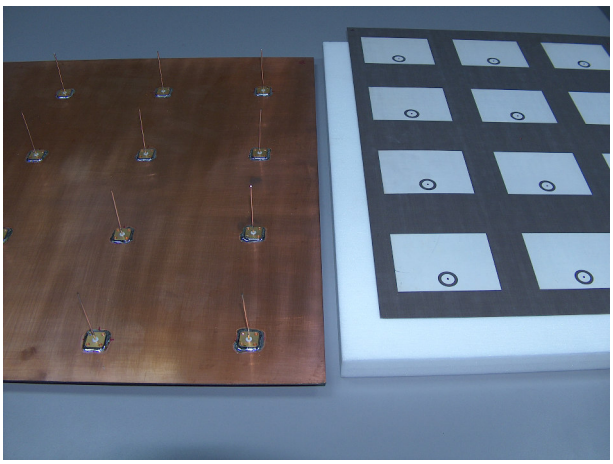

**Fig. 2.10.** Ring slotted patch array for Landslides Early Warning Application during the fabrication

In Tab. 2.2 are outlined the main geometrical parameters of each fabricated module. Since radar antenna has been designed for an outdoor application, copper radiating elements have been covered by a thin silver film in order to preserve them from oxidation processes. A photograph, showing the two modules, once assembly was completed, is provided in Fig. 2.11.

**Table 2.2.** Geometrical parameters of horizontal polarized ring slotted antenna array

| Parameter | Value [mm] |
|---|---|
| Module Length | 400 |
| Module Width | 400 |
| Vertical distance between edges | 28 |
| Horizontal distance between edges | 45 |
| Number of radiating elements | 16 |
| Adhesive thickness | 0.038 |
| Support substrate thickness | 0.762 |
| Fiberglass Thickness | 1.6 |
| Foam Thickness | 20 |
| Copper thickness | 0.036 |

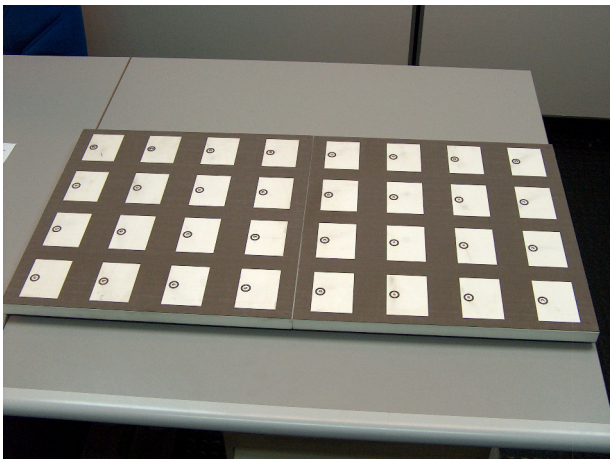

**Fig. 2.11.** Ring slotted antenna array: fabricated modules after assembly

Another important aspect involving the design of the final array concerns feed network. In particular, the feed network has been provided by two commercial power dividers with 16 output ports and input connected trough coaxial cables to a smaller power divided where input is in turn connected or to the circulator (in the configuration using only one antenna in both transmission and receiving path, see 2.3) or directly to the receiving path (in this case a standard 20dB gain Horn was used for transmission). The realized feeding network is shown in Fig. 2.12.

**Fig. 2.12.** Ring slotted antenna array: feed network

As shown in Fig. 2.12, an iron shell (painted in white) has been realized in order to fasten the three power dividers and the array to the engine used for angle scanning (which is directly controlled by the Software Defined Radar). A plexiglass cornice has been used to secure the two modules to the shell. For preserving connections and feed network from atmospheric agents, all the edges of the iron shell are in turn covered by thin plexiglass sheets. Before being integrate in the complete radar system, the ring loaded patch array has been tested in the anechoic chamber of Microwave Lab at University of Calabria. Return Loss measurements have been carried out on the prototype, and results have been provided in Fig. 2.13.

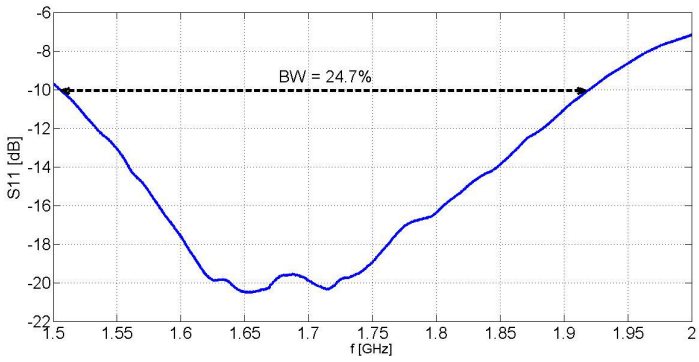


**Fig. 2.13.** Ring slotted antenna array: Measured Return Loss

Measured Return Loss further validate the wideband behavior obtained by radar antenna prototype fabricated following the design technique proposed in this work. In particular, a bandwidth of 24.7 %, respect to the central frequency, has been successfully obtained. In Fig. 2.14 a photograph showing an E-Plane far field test at the central frequency 1.8GHz is provided, while, radiation pattern at the central frequency 1.8GHz is shown in Fig. 2.15.

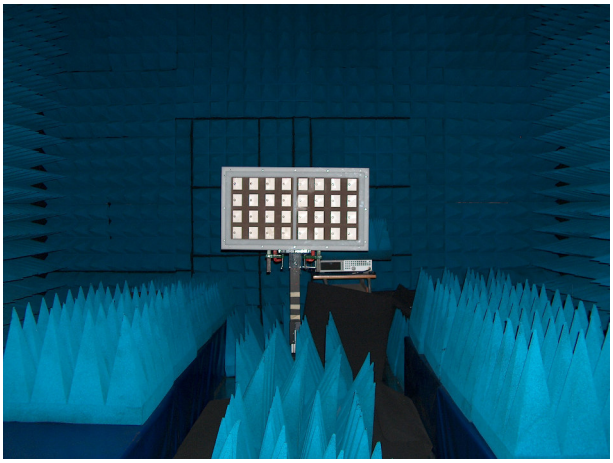

**Fig. 2.14.** Ring slotted antenna array during a Far Field test @ 1.8 GHz

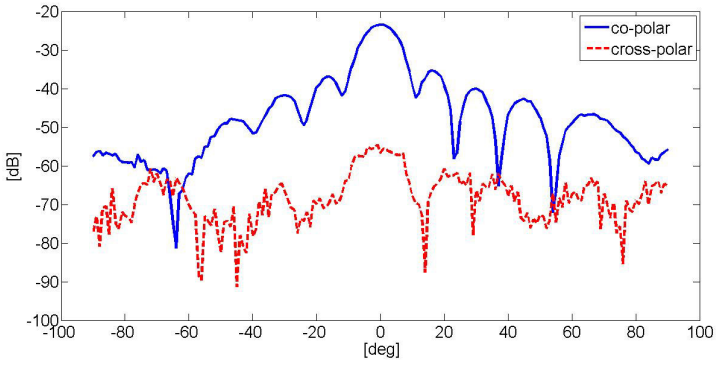


**Fig. 2.15.** E-Plane Far field measurements of ring slotted antenna array @ 1.8 GHz

A series of measurements for both E-Plane and H-Plane at different frequencies have been carried out, substantially showing the same results achieved in simulations. In particular, the same bandwidth, the same behavior

of cross-polar field component and the same beam width in both E-Plane and H-Plane have been obtained, further validating the correctness of the design. In the final step, L-Band radar antenna has been integrated into the complete radar system and different indoor and outdoor test have been successfully carried out. A photograph of the complete scheme during a preliminary test is provided in Fig. 2.16.

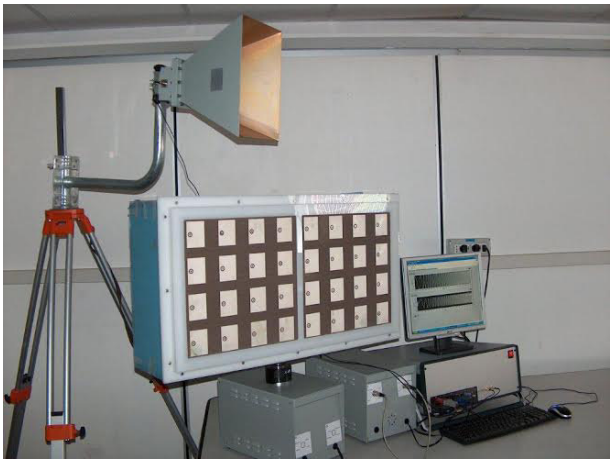

**Fig. 2.16.** L-band Ring Slotted Antenna Array integrated in the Software Defined Radar for Landslides Early Warning

## 2.3 Dual Polarized Ring Loaded Patch Array for Multi-Mode and Multi-Frequency Airborne Radar Design

### 2.3.1 System Description

In the last ten years, great interest has been devoted to the development of airborne radars working in the frequency range from VHF/UHF to L band (e.g. see [41, 42, 43, 44, 45] ). The combination of low frequencies and high relative bandwidth of such systems allows several military and civilian applications. Glaciers investigation, which is one of the main possible application of the proposed design, represents an attractive field for airborne radar systems working at these frequencies. In [46], for instance, an interesting analysis of the ice sounder signal in the presence of azimuth slopes has been performed at P-Band frequencies, while in [47] airborne experiments using 150MHz and 450MHz radars have been carried out to measure ice thickness on the Greenland ice sheet, obtaining the basal topography and the physical properties of the glacier bed.

The work in which a single polarized and a dual polarized ring slotted antenna are integrated in, deals with the design of multimode/multifrequency airborne radar suitable for imaging and subsurface sounding. In particular, the radar has been completely designed by the research team CO.Ri.S.T.A.(and promoted by Italian Space Agency (ASI) ) for what concerns the RF and the electronic aspect, and by the University of Calabria for what concerns the design, realization, and test of SAR antennas (designed starting by the concepts provided in this work). The system operates at relatively low frequencies in the range from VHF to UHF: the low one (163MHz), has been used in sounder mode, while the middle and high UHF frequencies (450MHz and 860MHz) are currently used in SAR configuration, but pointing the antennas at nadir; also, sounder configuration is in principle possible.

The entire system can be schematized as built by three main blocks (Fig. 2.17): Radar Digital Unit (RDU), Radio Frequency Unit (RFU), and Power supply Unit (PSU). The RDU is in charge of the parameters setting, timing generation, and data handling. It is a full programmable digital unit comprising the Analog to Digital Converter (ADC) and the data storage unit. The RFU embeds the Frequency Generation Unit (FGU), having the task to generate all synchronizations and RF signals, and the DSP, which generates the Low Frequency Modulated (LFM) signal chirp by means of digital synthesis. The PSU provides the power supply to the whole system by external 28V DC voltage.

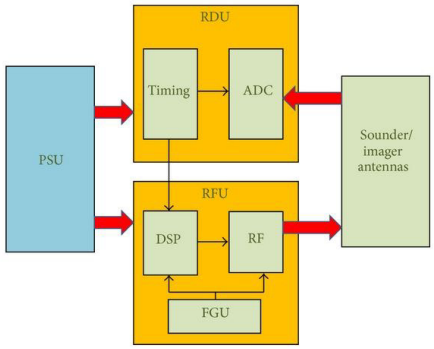


**Fig. 2.17.** Block diagram of the radar system

The general architecture of the system is depicted in Fig. 2.18. As it can be seen, the design is conceived so that most building blocks are shared by sounder and imaging modes. In particular, base band signal generation, base band data sampling, and data handling are common to both sounder and imaging operational mode. This represents the main feature of the entire system, so the possibility to switch the frequency band and other parameters on

the fly permit a very high adaptability of the system to different scenarios, allowing also a significant reduction of the costs and the time due to experimental tests. Another great advantage stands in the utilization of the same ADC, which is possible due to the adoption of an under-sampling technique.

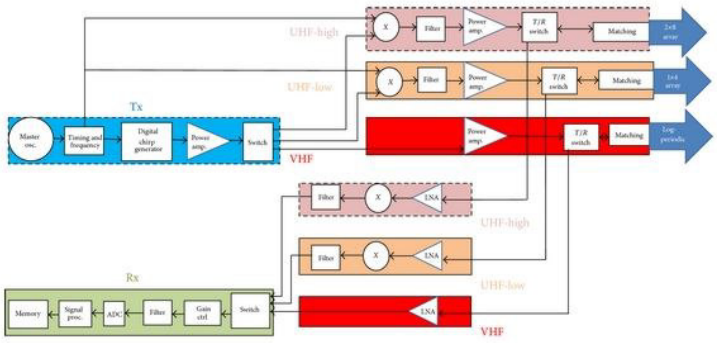


**Fig. 2.18.** General architecture of the radar system

The system has been designed to be very flexible as far as timing and configuration parameters are concerned. Stepped frequencies and bandwidth are generated by means of DDS technology and all relevant parameters can be configured by the user before the flight. Therefore, the system has the capability of easily changing the frequency values and overlapping the bandwidth as well. The system settings for the different functional modalities are described as follows:

Sounder mode: transmitted bandwidth of 10 MHz centered on a 163 MHz carrier. The transmitted signal is generated by FGU as LFM with the starting frequency at 158 MHz.

SAR-Low: stepped 40 MHz transmitted bandwidth synthetized by four sub-bands of 10 MHz transmitted over four carriers. The carriers differs of 10 MHz each other, thus no overlap arises between the transmitted sub-bands. By considering the four frequency sub-ranges, the transmitted signal covers the frequency range [430-470] MHz.

SAR-High: stepped 80 MHz transmitted bandwidth synthesized by eight sub-bands of 10 MHz transmitted over eight carriers. The carriers differ of 10 MHz each other, thus no overlap arises between the transmitted sub-bands. By considering the four frequency sub-ranges, the transmitted signal covers the overall frequency range [820-900] MHz.

The designed architecture allows a high flexibility to the system in terms of transmitted bandwidth; in fact, the radar can be easily upgraded to transmit a wider bandwidth, so a large operative bandwidth becomes a fundamental feature for SAR antennas integrated in the system. The radar has been in-

stalled on a civil helicopter and its operation has been validated in flight in both sounder and imager mode. Three different antennas are adopted: one for the sounder and two for the imager mode. The sounder antenna is a standard Log periodic with four radiating elements, having a 7dB gain, a beam width of 68 degrees, and a front-to-back ratio of 19dB, while in the imager mode, as outlined below, two different antenna arrays, composed of ring slotted patch antennas, have been designed in the way outlined in Subsection 2.3.2 and Subsection 2.3.3 of this thesis.

### 2.3.2 450 MHz Vertical Polarized Ring Slotted Antenna Array: Design and Experimental Results

Following the design technique proposed in Section 2.1, a vertical polarized Ring Slotted antenna, working in the low-UHF operative frequency range of the airborne radar has been simulated, fabricated and tested in the Microwave Lab at University of Calabria. In particular, for SAR-Low Imager Mode, a 40 MHz bandwidth has been required, but, in order to guarantee the use of the same architecture according to new possible features, a larger bandwidth had to be achieved. According to Fig. 2.1, total dimensions of P-Band single element are defined in Tab. 2.3. Radiating elements and ground-plane are composed by copper sheets, a foam substrate and a support substrate of Arlon Di-Clad 870 have been used, and a fiberglass sheet has been located under the ground-plane for robustness reasons, exactly in the same way for the fabrication of L-Band Antenna for Landslides Early Warning Application.

**Table 2.3.** Geometrical parameters of P-Band vertical polarized ring slotted antenna single element

| Parameter | Value [cm] |
|---|---|
| Ground Plane Length | 40 |
| Ground Plane Width | 40 |
| Patch Length | 30 |
| Patch Width | 24 |
| External Ring Radius | 3.8 |
| External Ring Radius | 2.3 |
| Feed Point Coordinates | ( 0, -7) |
| Foam Height | 6 |
| Support Substrate Height | 0.0762 |

A 4x1 array antenna has been successively designed. The fabrication process was the same used for the antenna integrated in the Landslide Early Warning, described in Section 2.2, while, a light and compact polycarbonate

cover has been designed and fabricated in order to fasten the four modules composing the array to the supporting structure integrated in the helicopter used for flight test. In particular, the dimension of the entire array structure, included the protection for the elements, are outlined in Tab. 2.4.

**Table 2.4.** Geometrical parameters of horizontal polarized ring slotted antenna array

| Parameter | Value [cm] |
|---|---|
| Total Length | 48 |
| Total Width | 168 |
| Vertical distance between edges | 10 |
| Horizontal distance between edges | 16 |
| Number of radiating elements | 4 |
| Adhesive thickness | 0.038 |
| Support substrate thickness | 0.0762 |
| Fiberglass Thickness | 0.16 |
| Foam Thickness | 6 |
| Copper thickness | 0.0036 |

Total structure has been fed using a commercial four way power divider, illustrated in figure Fig. 2.19, while the design of the polycarbonate protection around the array is provided in Fig. 2.20.

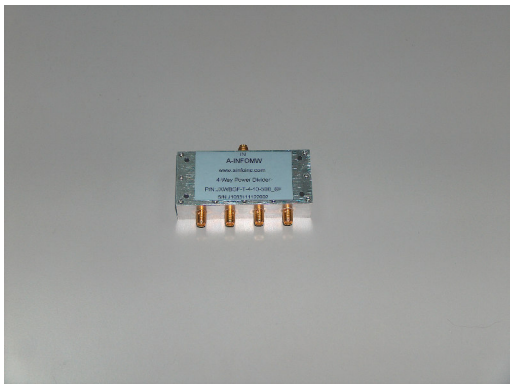

**Fig. 2.19.** Four way power divider feeding the vertical polarized ring slotted array

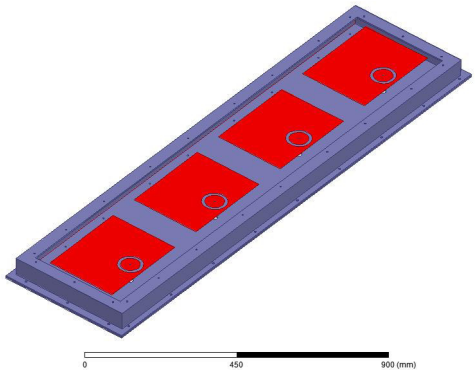


**Fig. 2.20.** Polycarbonate protection of the vertical polarized ring slotted array

The fabricated array has been tested in the anechoic chamber in Microwave Lab at University of Calabria before being integrated into the Multi-mode Multi-frequency airborne radar. A comparison between simulation and measured return loss of the P-Band ring slotted antenna array is shown in Fig. 2.21.

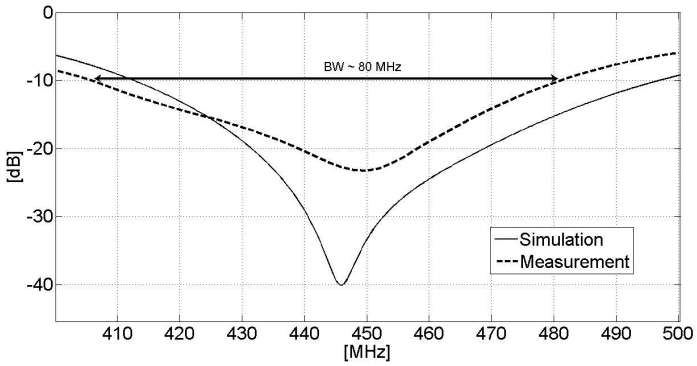


**Fig. 2.21.** Vertical polarized ring slotted array: simulated and experimental result comparison

A good agreement between simulated and measured return loss has been achieved,thus validating both the design technique and the fabrication process. Bandwidth is about 80 MHz, corresponding to 17% of the central frequency, much larger than classic microstrip patch antenna and greater than the one required for airborne radar features. A full characterization of the antenna array has been carried out also in terms of radiation pattern measurement,

a photograph of P-Band SAR antenna array during a far field test has been shown in Fig. 2.22.

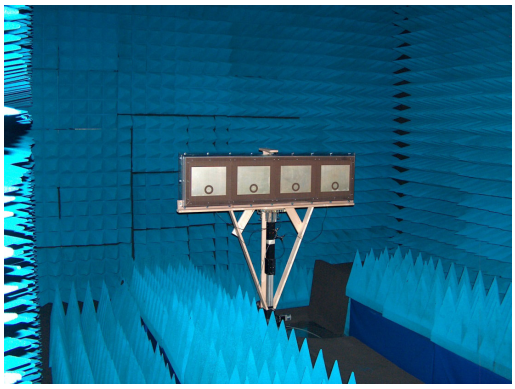

**Fig. 2.22.** SAR antenna mounted into the anechoic chamber at University of Calabria

In the same way of Landslides Early Warning L-Band array design described in Section 2.1, also in this case the main goal is the maintaining of cross-polar field components level under the co-polar one of a sensible value. A plot of co-polar and cross-polar far field components of the array in the H-Plane, at the central frequency of 450MHz,have been provided in 2.23.

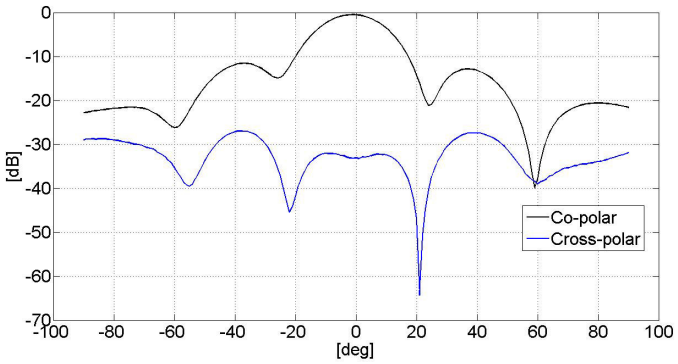


**Fig. 2.23.** Measured radiation pattern of SAR antenna: co-polar and cross-polar components @ 450 MHz

The array shows an excellent performance in terms of cross-polar component, which is significantly lower with respect to the co-polar one. Measurements on the E-Plane show the same performance. A -3dB beamwidth

approximately equal to 22 degrees, as imposed by the constraint on the azimuth resolution of Airborne Radar, is obtained in the co-polar H-Plane field. The radiation performances of the designed array is maintained all over the operating frequency range, as demonstrated by a very similar behavior of the measured radiation patterns at different frequencies, as shown in test results in the range [420-470]MHz reported in 2.24 for far field in H-Plane.

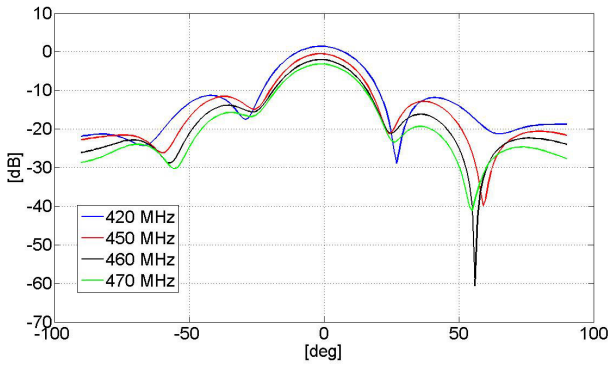


**Fig. 2.24.** Measured radiation pattern of SAR antenna: co-polar components at various frequencies, normalized respect to the one measured at 450 MHz

The radiation performances at different frequencies in the operating bandwidth maintain a very similar behavior, both in terms of radiation shape (the beamwidth is about 22 degrees for each component) and peak value, performing a wide -3dB frequency bandwidth suitable for an hypothetical extension of the Multimode and Multifrequency radar features. For a further validation, a measurement of the peak gain at the broadside direction has been performed, and it is shown in Fig. 2.25.

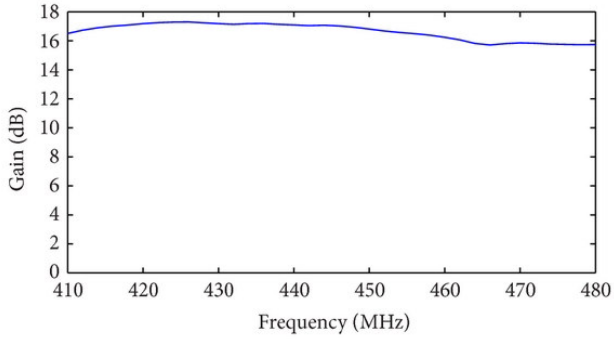


**Fig. 2.25.** Measured gain of SAR-Low antenna versus frequency at boresight

Gain of the antenna array is maintained between 16 dB and 18 dB all over the operative frequency range of the radar, performing a -3dB bandwidth larger than 20 %, surprisingly higher than the one performed by both classic patch antenna and most of typical slotted configuration. Imager SAR antenna, with vertical polarization, has further integrated to the RF and electronic part of the radar developed by CoRiSTA, which mounted the entire system on a civil helicopter (Eurocopter AS350) for a flight test. A photograph of the developed system during the flight campaign is shown in Fig. 2.26.

**Fig. 2.26.** Imager P-Band SAR antenna in flight configuration

Several sounding and imaging tests were successfully carried out by CoRiSTA, but their discussion lie outside the aim of this thesis work. However, a final image of SAR obtained over a coastal zone in Southern Italy (Paestum) analyzed in the flight campaign, compared to a photograph of the area, has been provided in Fig. 2.27.

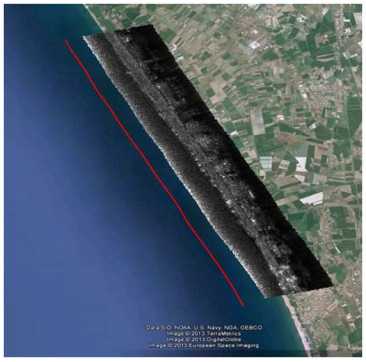

**Fig. 2.27.** SAR image obtained over a coastal zone in Southern Italy (Paestum)

Supplementary test on Multi-Mode Multi-Frequency Airborne radar completely validated the correctness of both RF and electronic part of the radar system and the vertical polarized P-Band ring slotted antenna array. A later stage was the integration of a 900 MHz array, composed of the dual polarized ring slotted antenna design provided in Section 2.1, into the airborne radar in order to complete the UHF-High TX-RX channel path. Design, fabrication and test of this antenna are provided in Section 2.3.3 of this work.

### 2.3.3 900 MHz Dual Polarized Ring Slotted Antenna Array: Design and Experimental Results

Ring slotted microstrip patch antenna has been properly modified, how outlined in Section 2.1, in order to support dual polarization. Layout proposed in Fig. 2.2 permits to achieve the same characteristics of a single polarized ring slotted antenna, both in terms of return loss and radiation pattern, without a significant complication of the basic geometrical model, and without preventing compactness and robustness due to a single layer flat layout, suitable for radar applications. In order to achieve significant results, the currents causing the two polarization (when the channel related to the other polarization is not fed), have to be equal in intensity and 90 degrees shifted in the plane of the antenna, so, looking to Fig. 2.2, the patch must be square, the dimension of the two annular slot must be equal and there must be the same distance between the center of the patch and the two feeding point, so in this case, fields

due to horizontal polarization are completely identical to the one produced by the vertical one, allowing the correct features of the UHF-High channel of the airborne radar. Referring to Fig. 2.2 , the main geometrical parameters of the single elements composing the dual polarized ring slotted antenna array is outlined in Tab. 2.5.

**Table 2.5.** Geometrical parameters of dual polarized ring slotted antenna single element

| Parameter | Value [mm] |
|---|---|
| Elementary Cell Length | 200 |
| Elementary Cell Width | 200 |
| Patch Length | 118 |
| Patch Width | 118 |
| External Ring Radius | 14.3 |
| Internal Ring Radius | 11.2 |
| V-Pol Feed Point Coordinates | ( 0, 26.8) |
| H-Pol Feed Point Coordinates | (-26.8,0) |
| Foam Height | 30 |
| Support Substrate Height | 0.762 |

For practical reasons, four identical modules of 2x2 dual polarized ring slotted antennas have been designed, fabricated and assembled in order to compound a 2x8 overall array (160 x 40 mm). The fabrication process is identical to the one used for the two single polarization array proposed in this Chapter, obviously, the only significant difference deals with the feeding network, where, each channel is connected to a proper 16-ways power divider. In order to maintain the same features, power dividers and connectors have been chosen identical for both polarization. A photograph of the single 2x2 module is provided in Fig. 2.28.

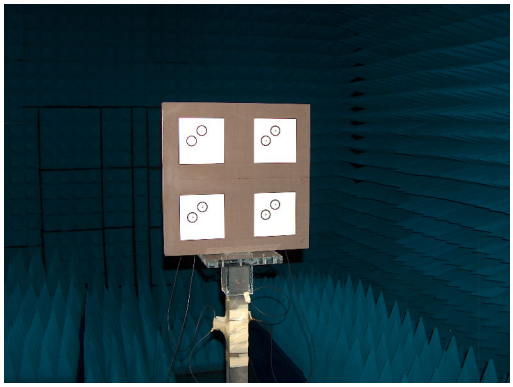

**Fig. 2.28.** UHF-High dual polarized ring slotted antenna prototype

A single module of UHF-High dual polarized ring slotted antenna prototype is identical in dimension to a single element used in the UHF-low design, so the resulting overall arrays are identical too, in order to an easier interchange and integration into the radar system support on the civil helicopter used for the test. Each module has been tested in both Return Loss and Radiation pattern. In particular, each single return loss element,each coupling coefficient with the other polarization port, and each transmission coefficient towards the other nearest port with the same polarization, have been measured in the 2x2 module, closing the port not involved in the test on a matched load. Return Losses related to the two polarization of the single antenna element are provided in Fig. 2.29, while the isolation between the two polarization is defined in Fig. 2.30.

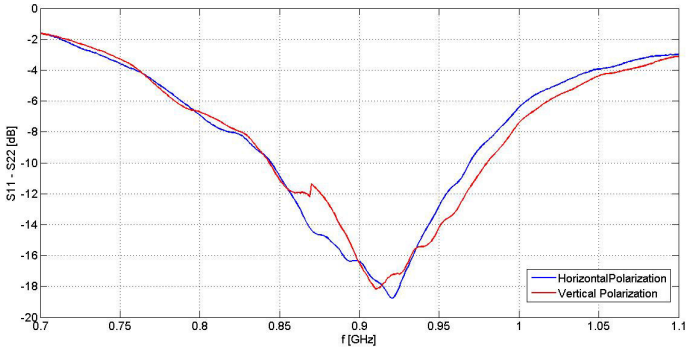


**Fig. 2.29.** Single element Return Loss measurements of UHF-High dual polarized prototype

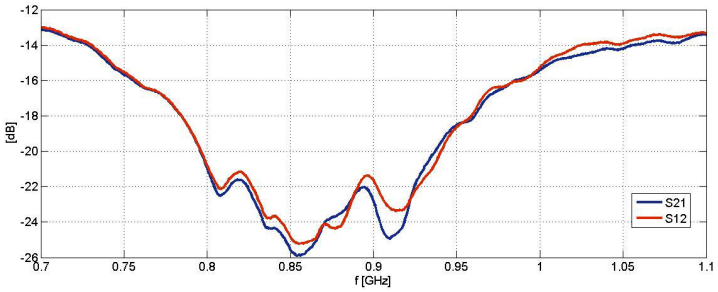


**Fig. 2.30.** Single element isolation between polarization measurements

Also in this case, as emerged during return loss measurements of the single polarized antenna, a large bandwidth behavior, around 15 %, has been achieved. Since a flat behavior of the transmission coefficients between the two ports feeding the single element has been measured in the overall frequency range, a good level of isolation between the two polarization is assured. Due to the axial symmetry of the antenna, all the results measured are almost identical for both polarization, thus validating both the design and the fabrication process. The entire SAR High antenna array prototype has been tested in the anechoic chamber at University of Calabria, a photograph during far field measurements is shown in Fig. 2.31.

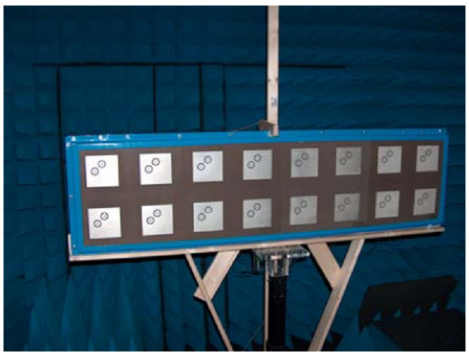

**Fig. 2.31.** SAR-High antenna mounted into the anechoic chamber at University of Calabria

Measured co-polar and cross-polar field components in the H-Plane (feeding the array for obtaining horizontal polarization) at the central frequency of 900MHz are shown in Fig. 2.32.

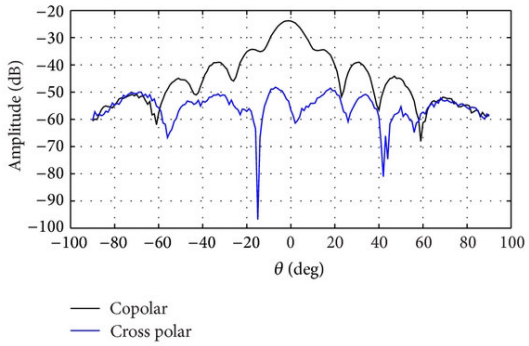


**Fig. 2.32.** Far Field measurement at the central frequency @ 900MHz

A -3dB beamwidth of about 12 degrees, imposed by the constraints on the azimuth resolution of UHF-high mode of the radar, can be observed in the co-polar field and low lateral lobes have been obtained. Also in this case, co-polar field components significantly above ( more than 25dB) the undesired cross-polar components have been achieved. In order to further validate the correct behavior of the array in the overall operative frequency range, far field measurements have been repeated for different frequencies and for both polarization. In Fig. 2.33 the measured gain for both polarization at the broadside direction have been shown.

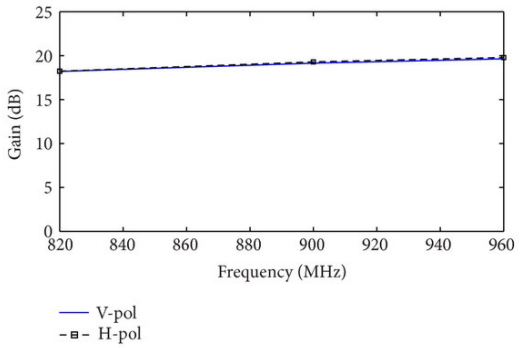


**Fig. 2.33.** Gain measurements for different frequencies: comparison between vertical and horizontal polarization

The measured gain is approximately identical for vertical and horizontal polarization and maintains a flat behavior in the overall frequency band, with a peak value in the broadside direction between 17dB and 20dB, thus further

confirming the wideband behavior of the proposed antenna. The complete array has been integrated into the airborne radar and has been employed into two different flight test for Landscape monitoring, the first one, briefly described in Section 2.3.2, in which a civil Helicopter (Eurocopter AS350) has been used for measurement, and the second one, in which the entire system has been transported on a military helicopter (see Fig. 2.34).

**Fig. 2.34.** Dual polarized SAR antenna mounted on a military helicopter for a flight campaign

# 3

# Wideband Fabry Perot Cavity Antenna, Based on Metasurfaces, for Radar Applications

## 3.1 Fabry Perot Cavity Antennas

A FabryPerot interferometer is a structure, consisted of two highly reflecting mirrors facing each other, that was developed at the beginning of last century by the French physicians Charles Fabry and Alfred Perot [48]. The device, based on multiple reflection of waves between two closely spaced and different shaped reflecting mirrors (see Fig. 3.1) , has been widely employed in optical physical for producing high field intensities with low input powers, for dichroic filters, laser resonators, and they can be used to prolong the interaction length in laser absorption spectrometry.

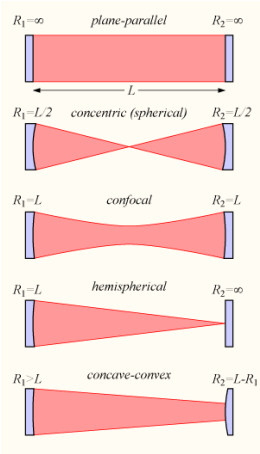


**Fig. 3.1.** Fabry Perot Cavities

The first application of Fabry Perot Cavities in antenna field was carried out in 50's by Von Trentini [49] , who placed a Partially Reflective Surface

(PRS) in front of a grounded antenna in order to achieve a gain enhancement. He evaluated the behavior of multiple reflections between the ground plane and the PRS, and then derived an expression for the resonance condition that yields maximum radiated power at broadside, assuming the PRS consisted of an array of closely spaced parallel conducting wires oriented parallel to the electric field. These typology of antennas are also classified as leaky wave antennas, because the enhanced directivity is based on the excitation due to a single radiating element of a leaky wave along the antenna geometry, whose basic scheme is shown in Fig. 3.2. From the ray viewpoint, an electromagnetic wave excited by the source is bounced in the FPCA, so, in order to superpose in phase, the phase shift of the EM waves at each return is an integer multiple of $2\pi$, so, when the reflection coefficient of both mirrors is equal to -1, the total length of the cavity must be a multiple of an half-wavelength.

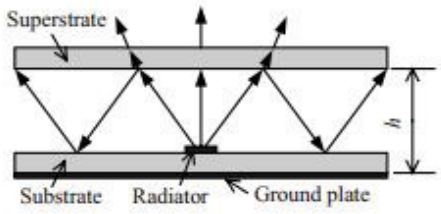


**Fig. 3.2.** Fabry Perot Cavity Antenna: Basic Layout

The first chapter book dedicated to this topic was provided by Tamir [50] in 1969, while another important work was reported by Oliver in [51]. Similar structure have been widely studied in literature, significant analysis have been done in [52], in which a Fabry-Prot resonant-cavity antenna using a single high-permittivity superstrate as the PRS have been outlined, and in [53], where layers that alternate low and high permittivities have been employed. In the last twenty years several studies have been carried out, especially after the concept of metamaterial and metasurface have been exploited [54, 55, 56]. In particular, the Electromagnetic Band Gap (EBG) phenomenon has been widely analyzed in the recent literature as superstrates for antennas to achieve gain enhancement, using homogeneous structures combined each other [57, 58], or employing more complex metamaterials with a periodicity along the longitudinal and transverse directions [59, 60, 61, 62, 63]. In Fig. 3.3 is shown how a 3D metamaterial structure, composed by thin rods along E-Field direction, acts as a superstrate for improving antenna directivity.

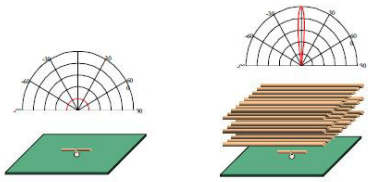

**Fig. 3.3.** EBG structure for antenna directivity enhancement

In 2001, an improved version of Trentini antenna has been developed recently by Feresidis and Vardaxoglou [64] integrating a waveguide into the structure and analyzing different PRS, respectively composed by slots, dipoles, rings and patches. Recently, following van Trentini ray theory analysis and using PRS with a proper reflection coefficient, several works on thin cavities have been implemented [65, 66], often using Artificial Magnetic Conductors (AMC) in order to achieve a zero phase reflection over a narrow frequency band, half-sizing the necessary path in the cavity to achieve coherent interference between waves allowing radiation [67, 68, 69]. Since one of the most annoying limitation on Fabry Perot Cavity Antennas is related to the narrow bandwidth, some recent studies are oriented to enlarging the operative frequency range using a multilayer configuration which allow an anomalous phase reversion of the normal path of the waves. The dual layer PRS composed by square patches on a dielectric slab deeply analyzed in this Chapter, has been studied in [70], where a broadband high-gain 2-D Fabry-Perot leaky-wave antenna, with a peak gain of 18 dB, has been presented. While our work has been mainly focused on the synthesis of the PRS, in [70] a Full-wave method of moments (MoM) have been employed for a simple and effective estimation of the near fields upon plane wave illumination and the extraction of the far field directivity and radiation patterns of the antenna, achieving a 11 % bandwidth . The most recent work in literature on this topic has been outlined in [71], where a broadband Fabry Perot Cavity, with a peak gain of 13dB, composed by multilayer EBG structures, has been outlined.

## 3.2 Open Resonator Theory and Wave Analysis by Parabolic Approximation

Most of analysis techniques of Fabry-Perot Cavity Antennas are based on simple ray tracing or equivalent transmission circuits, considering fields in the cavity propagating as a planar wave. Following this assumptions, geometrical dimensions of the ground-plane and PRS are considerate infinitely extended and higher order mode propagation are neglected, so, while in the field calculation outside the cavity they represent an easy and affordable way, for the

design of the cavity mirror themselves they don't provide good results, especially because of the extreme sensitivity of the length of the cavity on antenna performances. In this work, an equivalent transmission network has been provided for synthesize a Fabry Perot Cavity Antenna design (see Section 3.4), but part of the circuit has been built using Method of Moment analysis and the propagation inside the cavity has been assumed correcting the phase of reflection coefficient with the analysis of open resonators by parabolic approximation of the wave equation. A parabolic equation was first introduced into the analysis of electromagnetic wave propagation by Leontovic in [72]. In particular, it is an approximation of the wave equation valid when the operative wavelength is enough smaller than the other geometrical parameters of the structure. A field component $U$ of a coherent wave satisfies the scalar wave equation:

$$\nabla^2 U + k^2 U = 0 \tag{3.1}$$

where $k = \frac{2\pi}{\lambda}$ is the propagation constant in the medium. Considering a complex exponential time dependence, field components can be expressed as

$$U = \Psi(x, y, z)e^{-jwz} \tag{3.2}$$

where $\Psi$ is a slowly varying function which represents the deviation from a plane wave. If the second derivative of $\Psi$ respect the longitudinal direction $z$ can be neglected, one obtains:

$$\frac{\delta^2 \Psi}{\delta^2 x^2} \frac{\delta^2 \Psi}{\delta^2 y^2} - 2jk\frac{\delta \Psi}{\delta z} = 0 \tag{3.3}$$

which is called the parabolic approximation of the wave equation and admits solutions of the type:

$$\Psi = e^{-j(P(z)+\frac{k}{2q}R^2)} \tag{3.4}$$

where:

$$R^2 = x^2 + y^2 \tag{3.5}$$

The parameter P(z) represents a complex phase shift associated to the propagation of the beam along the z axis, q (z) is the complex parameter which describe the beam intensity with the distance r from the z axis. This analysis has been applied in [73] in order to calculate fields in a plate parallel open resonator. Assuming the simple case in which cavity mirrors are composed by two finite sheets of Perfect Electric Conductor (PEC) of size 2a x 2b and their distance is 2l, one can apply the condition u= 0 on the mirrors, and writing the solution of Eq. 3.3 as:

$$U = \Psi(x, y, z)e^{-jkz} - (-1)^q \Psi(x, y, z)e^{jkz} \tag{3.6}$$

where q is the longitudinal number. One can separate the two contributes due to transverse direction, writing:

$$\Psi = \Psi_a(x,z)\Psi_b(y,z) \tag{3.7}$$

with the first function $\Psi_a$ solving

$$\frac{\delta^2\Psi_a}{\delta^2 x^2} - 2jk\frac{\delta\Psi_a}{\delta z} = 0 \tag{3.8}$$

and the second one, $\Psi_b$, solving

$$\frac{\delta^2\Psi_b}{\delta^2 y^2} - 2jk\frac{\delta\Psi_b}{\delta z} = 0 \tag{3.9}$$

The eigenfrequency of the resulting mode is given by:

$$kl = \pi(\frac{q}{2} + p), p = p_a + p_b \tag{3.10}$$

where

$$p_a = \frac{m^2\pi}{4(M_a + \gamma + j\gamma)^2}, m = 1, 2.... \tag{3.11}$$

and

$$p_b = \frac{n^2\pi}{4(M_b + \gamma + j\gamma)^2}, \gamma = \zeta(\frac{1}{1}) = 0.824, n = 1, 2.... \tag{3.12}$$

where $\zeta$ is the Zeta Riemann function. The term $M_a$ is related to the width size $2a$ of the mirrors:

$$M_a = \sqrt{\frac{2ka^2}{l}} \tag{3.13}$$

and the term $M_b$ to their height $2b$:

$$M_b = \sqrt{\frac{2kb^2}{l}} \tag{3.14}$$

In dimensionless coordinates, imposing the transformation:

$$\begin{cases} \xi = \sqrt{\frac{k}{2l}}x \\ \mu = \sqrt{\frac{k}{2l}}y \\ \zeta = \frac{z}{2l} \end{cases} \tag{3.15}$$

one can write, for the even longitudinal modes:

$$u_e(\xi,\mu,\zeta) = 2e^{-jp\pi}f_a(\xi)f_b(\mu)cos(\pi p\zeta) \tag{3.16}$$

and, for the odd ones:

$$u_0(\xi,\mu,\zeta) = 2e^{-jp\pi} f_a(\xi) f_b(\mu) sin(\pi p\zeta) \tag{3.17}$$

where:

$$f_a(\xi) = \begin{cases} cos(\frac{m\pi\xi}{(M_a+\gamma+j\beta)}), \text{ for m odd} \\ sin(\frac{m\pi\xi}{(M_a+\gamma+j\beta)}), \text{ for m even} \end{cases} \tag{3.18}$$

and

$$f_b(\mu) = \begin{cases} cos(\frac{m\pi\mu}{(M_b+\gamma+j\beta)}), \text{ for m odd} \\ sin(\frac{m\pi\mu}{(M_b+\gamma+j\gamma}), \text{ for m even} \end{cases} \tag{3.19}$$

A rigorous extension of this analysis in a different structure, as the one studied in this work, could lead to very difficult solutions due to a complication of boundary conditions; however, using the solution of the paraxial approximation of the wave equation for characterizing propagation on longitudinal axis, and integrating the boundary condition with a reflection model calculated trough Method of Moments, an easy and general synthesis technique has been developed for more complicated cavities, and fully explained in Section 3.3.

## 3.3 Double layer Square Patches on Dielectric Slabs

### 3.3.1 Geometry

In 1999, Sievenpiper el al. [56] proposed a periodic metallo-dielectric structure, that exhibited a high impedance over a limited frequency bandwidth. This so called High Impedance Surface (HIS) was composed of metallic patch periodically displaced on a dielectric substrate and shorted to the metallic ground plane through via holes. The use of such structure in a Fabry-Perot Cavity allows a reduction of its total length, due to the fact that an HIS structure presents, over a relative narrow bandwidth, a near zero reflection phase for waves normally incident to the surface.

In order to describe resonant cavity modes, a simple optical ray model is usually considered [49] . Considering the multiple reflections of the wave emitted by the antenna, a resonance is obtained when the reflected waves are each other in phase after one cavity roundtrip. Resonant condition leads to:

$$h = \lambda\frac{\phi_{s2} - \phi_{s1}}{4\pi} \pm \frac{n\lambda}{2} - \sum_{i=1}^{N} t_i\sqrt{\epsilon_{ri}} \tag{3.20}$$

where $\phi_{s2}$ is the reflection phase of the partially reflecting surface which permits transmission of the free space , $\phi_{s1}$ is the reflection phase of the ground plane ( or an impenetrable HIS in implementations which use metasurfaces ) , $\epsilon_{ri}$ are the relative permittivity of eventually N additive substrates and $t_i$ their thickness, while $n$ is an integer qualifying the electromagnetic longitudinal mode of the cavity. According to Eq. 3.20, minimizing $\phi_{s2}$ or $\phi_{s2}$ one can minimizing cavity thickness.

The use of metasurfaces answers this purpose since they can exhibit an LC resonance. This resonance helps to have a reflection phase response varying from 180 degrees to -180 degrees, passing through 0 at the resonance frequency.By choosing a desired operating cavity frequency above the metasurface resonance, where the reflection phase is near zero, one could achieve a very low cavity thickness. However, Sievenpiper configuration is hardly to fabricate, due to the via holes, so, simple patches printed on a grounded substrate can be used to achieve the same effect, but in a more narrow bandwidth. The layout of the elementary cell is shown in Fig. 3.4.

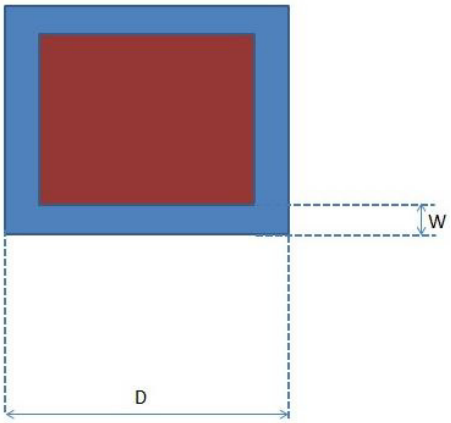


**Fig. 3.4.** AMC basic cell

In [75], simple analytical formulas are introduced for the grid impedance of electrically dense array, which can be used for both HIS reflection phase analysis and transmission phase analysis if an ungrounded patch array would be used as partially reflecting surface. For a better design of an AMC surface a procedure based on method of moment can be considered. In any case, even if the longitudinal size of the cavity can be significantly decreased, the bandwidth of the resonator, which is normally of a few percent of the central frequency, dramatically waste due to the extremely narrow bandwidth AMC operation. One of the main problem due to the introduction of an AMC surface of this type in a Fabry-Perot cavity is due to the extreme sensibility of the geometric parameters which assure a zero phase reflection. These two aspects make the fabrication of a Fabry-Perot Cavity antenna based on an AMC extremely difficult.

However, if the design of a wideband Fabry Perot Cavity antenna based on an AMC used in substituting of the ground plane is impossible, due to behavior itself of the AMC, the classical definition itself of 3D metamaterial (instead of a 2D metasurface) , applied to the square patch periodic struc-

ture can lead to interesting results in this context. In general, a metamaterial allows a left handed propagation of travelling waves, leading to the extraordinary condition in which Pointing vector S and the direction of propagation k are oriented in the opposite direction, causing an anomalous behavior in the dispersion diagram. In particular, natural phase decrease of propagation constant against the frequency can be delayed, or even completely reversed. Most of the revolutionary application of metamaterials are unfortunately limited by the reduced bandwidth in which a canonical bulky material can perform contemporary both negative permittivity and negative permeability. In our case, even if the AMC behavior of an array of patch on a dielectric grounded sheet is very narrow, the ungrounded version, which impedance is smoother, can be combined with another array (see Fig. 3.5) to form a secondary cavity used as Partially Reflective Surface [70] and allowing an anomalous phase reflection between primary and secondary cavity.

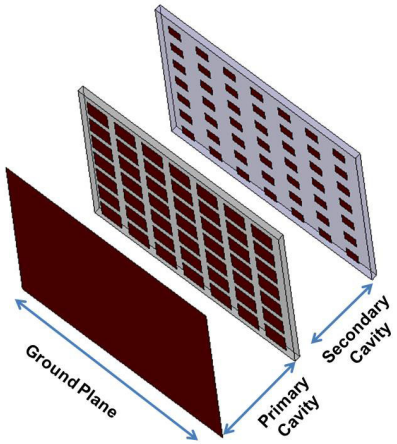


**Fig. 3.5.** Dual layer PRS acting as a bulky metamaterial inserted as a Fabry Perot Cavity mirror

In particular, it is interesting to see how this structure, without the claim to be a both negative permittivity and permeability material, allows a positive slope of phase reflection in a certain frequency range, which balance the natural phase decreasing of the waves traveling in the cavity, acting just in the same way like causing a discontinuity between air and a 3D bulky left handed metamaterial. Starting from the structure very recently proposed in [70], a novel synthesis has been carried out in order to find a simple design procedure for a wideband Fabry Perot Cavity antenna.

### 3.3.2 A novel synthesis technique for Phase Reversing Design

In classical Fabry Perot Cavity antennas, the most critical geometrical parameter, apart the extremely accurate alignment in fabrication phase, is the distance between cavity mirrors (in this case between ground plane and the first patch array plane). In most of the works this distance is calculated using a simple ray analysis, but some important aspects, like higher order propagation and finite mirrors surface area are usually neglected. A significant solution for finding resonant modes in a Fabry-Perot cavity, is given by the parabolic approximation of the wave equation (see Section 3.2).

As suggested in [73], an additional phase shift $\theta = 2p'\pi$, where $p' = Im(p)$ as calculated in Eq.3.10, should be considered in the longitudinal direction. Adding the phase delay, Eq.3.20 becomes:

$$h = \lambda\frac{\phi_{s2} - \phi_{s1}}{4\pi} \pm \frac{n\lambda}{2} - \sum_{i=1}^{N} t_i\sqrt{\epsilon_{ri}} - p'\lambda \tag{3.21}$$

Replacing Eq. 3.11 and Eq.3.12 in Eq. 3.10, $p$ can be rewritten as

$$p = p_a + p_b = \frac{m^2\pi}{4(M_a + \gamma + j\gamma)^2} + \frac{n^2\pi}{4(M_b + \gamma + j\gamma)^2} \tag{3.22}$$

In order to simplify the calculation, let consider the case of square walls,so $a = b$ and $M_a = M_b$ ; after few calculations one can isolate imaginary part of p:

$$p' = \frac{\pi}{4}(\frac{M_a + \gamma}{(M_a + \gamma)^2 + \gamma^2})^2(m^2 + n^2)^2 \tag{3.23}$$

And, in this case,adding the correction due to paraxial approximation, resonance condition becomes:

$$h = \lambda\frac{\phi_{s2} - \phi_{s1}}{4\pi} \pm \frac{n\lambda}{2} - \sum_{i=1}^{N} t_i\sqrt{\epsilon_{ri}} - \frac{\lambda\pi}{4}(\frac{M_a + \gamma}{(M_a + \gamma)^2 + \gamma^2})^2(m^2 + n^2)^2 \tag{3.24}$$

Now, in order to have a starting value for $h$ which can be used in a more accurate analysis, one can consider $M_a$ greater enough than $\gamma$ ,in this case Eq. 3.24 becomes:

$$h = \lambda\frac{\phi_{s2} - \phi_{s1}}{4\pi} \pm \frac{n\lambda}{2} - \sum_{i=1}^{N} t_i\sqrt{\epsilon_{ri}} - \frac{\lambda\pi}{4(M_a + \gamma)^2}(m^2 + n^2) \tag{3.25}$$

After few calculations, once replaced Eq.3.13 in Eq.3.25, one obtain a starting design value for a square mirrors Fabry Perot Cavity antenna:

$$h = \frac{\lambda\frac{\phi_{s2} - \phi_{s1}}{4\pi} \pm \frac{q\lambda}{2} - \sum_{i=1}^{N} t_i\sqrt{\epsilon_{ri}}}{1 + \frac{\lambda^2}{32a^2}(m^2 + n^2)} \tag{3.26}$$

Equation 3.26 can be considered as a correction of Eq. 3.20, considering a generic paraxial solution propagating in the cavity instead of a planar wave and considering both longitudinal and transverse modes. Obviously, in the case of an air filled classical Fabry-Perot cavity composed by two PEC conductors ($\phi_{s1} = \phi_{s2}$), the first cavity mode occurs when cavity thickness is exactly an half-wavelength.

Starting from this formulation, but using a step by step procedure based on Method of Moments and using the structures outlined above, a small lateral sized Fabry-Perot cavity can be easily designed. In first analysis, a distance $h_1$ between the PRS composed by the first of the two metamaterial sheets and the metallic ground plane has been considered like in Eq. 3.25. The same starting value for the distance $h_2$ between the two plates, which can be considered as the longitudinal length of the partially reflecting surface cavity, has been chosen. For both arrays a starting value of 0.4 wavelengths has been chosen as lattice period, according to what suggested in [74] for infinite array analysis in wideband reflectarray design. Initial distance between patches has been determined in order to avoid problems in terms of cutting tolerance of the milling machine. The analysis has been carried out in order to maximize the range in which the reflected phase, observed in a point near the ground plane, remains as constant as possible around the value $\phi_r = \pi$ in order to preserve resonance condition for a wideband behavior. In particular, MoM has been used to find the reflection coefficient in proximity of the PRS, and it has been inserted in a simple transverse equivalent network to evaluate the phase near the ground plane, as expressed in Fig. 3.6.

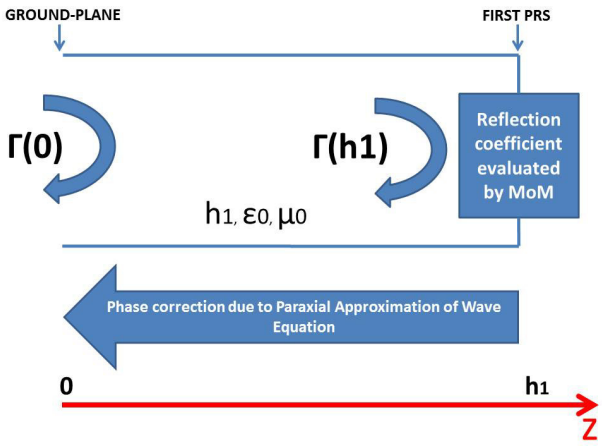


**Fig. 3.6.** Equivalent circuit for phase optimization

In this case, the analysis has been performed correcting the path between the meta-material like PRS structure and the ground plane with the additive

phase shift given by the solution of the parabolic approximation of the wave equation. Total phase delay between PRS and ground-plane can be calculated as:

$$\phi_r = \beta h_1 + 2\pi p' \tag{3.27}$$

Replacing Eq. 3.23 in Eq.3.27 , one obtains:

$$\phi_r = \beta h_1 + \frac{\pi^2}{2}(\frac{M_a+\gamma}{(M_a+\gamma)^2+\gamma^2})^2(m^2+n^2)^2 \tag{3.28}$$

where $M_a = 2a\sqrt{\frac{\beta}{h_1}}$ . Now, being $\Gamma(h_1)$ the reflection coefficient evaluated with the infinite array analysis through Method of Moment (and $h_1$ calculated like in Eq. 3.26), for evaluating the phase behavior $\Gamma(0)$ near the ground plane, one can consider the following expression:

$$\Gamma(0) = \Gamma(h_1)e^{-2j\phi_r} \tag{3.29}$$

which finally leads to:

$$\Gamma(0) = \Gamma(h_1)e^{-2j\beta h_1}e^{-j\pi^2(\frac{M_a+\gamma}{(M_a+\gamma)^2+\gamma^2})^2(m^2+n^2)^2} \tag{3.30}$$

Now, Eq. 3.30 represents the reflection coefficient of the metamaterial like structure near the ground plane. Notice that the first exponential term is due to a planar wave propagation and the second one is the additive phase shift due to generalization of the solution of wave equation. In fact, one can notice how, if infinite mirrors are selected, $M_a \to \infty$ and the second exponential term decay, indicating the propagation in the structure of a planar wave. Obviously, in a design procedure, maximizing the frequency range in which $\Gamma(0) \approx \pi$ one can maximize the bandwidth of the Fabry-Perot Cavity Antenna. In this formulation, one can observe how a positive slope of PRS phase reflection is not sufficient for a wideband behavior, but the slope of the anomalous phase reflection has to be tuned with the distance between PRS and ground plane and with the transverse dimensions of the cavity. The smaller is the lateral dimension of the Fabry Perot Cavity and the larger is its longitudinal length , the more significant is the contribution of the phase shift on the path inside the cavity. Starting by this formulation, the design of a dual layer surface performing an anomalous behavior of the reflection coefficient, can be done easily changing the geometrical parameters of the arrays, the distance between them, and the distance between the first partially reflecting surface and the ground-plane, evaluating in a simple way the direct effect of these parameters on the operative bandwidth of the structure. In order to better clarify the proposed synthesis technique, a numerical example of a double layer structure, working at the central frequency of 14 GHz, has provided in Section 3.3.2.

### 3.3.3 Numerical results

Focusing on the meta-material like sheets design, and starting from the formulation described above, a compact lateral size, wideband, metamaterial surface for a Fabry-Perot Cavity Antenna, has been designed at the central frequency of 14 GHz. In first analysis, a variation of the distance between the two arrays $h_2$ has been considered in order to obtain a positive phase slope in the correct frequency range. The reflection phase coefficient variation at the coordinate $z = h_1$, predicted by MoM, thought Ansoft Designer simulations, has been shown in Fig. 3.7.

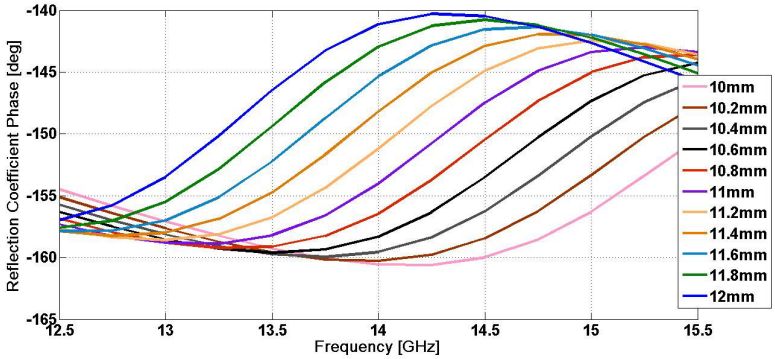


**Fig. 3.7.** Reflection coefficient phase in proximity of the first PRS, varying the distance between patch arrays

As shown in Fig. 3.7, a variation of the distance between patch arrays determines the frequency range in which the slope of the reflection phase assumes an extraordinary positive value. In order to evaluate in a more immediate way the best behavior of the reflection coefficient phase, equivalent circuit in Fig.3.6 and Eq. 3.26 have been used to evaluate the reflection coefficient phase near the ground plane. In Fig.3.8, is shown the variation of $\Gamma(0)$ considering a distance $h_1 = 10.7mm$ between the first metamaterial sheet and the ground plane, according to Eq. 3.26, and considering a very compact lateral size for the cavity, with $a = b = 55mm$, less than 3 times the relative free space wavelength.

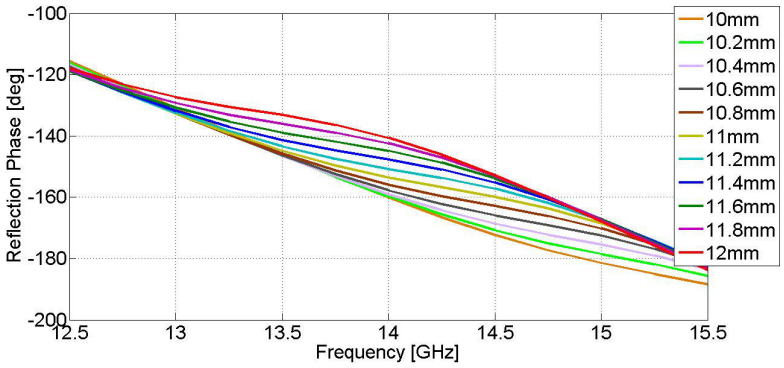


**Fig. 3.8.** Reflection coefficient phase transported near ground plane, varying the distance between patch arrays

Looking at Fig.3.8, one can see how the slope of these curves is smaller than the natural phase decreasing in a normal path. The flattest behavior near the central frequency 14 GHz is the one described by the curve for $h_2 = 11.6mm$. Using this last value, a tuning of the size of the first patch array element has been performed in order to find a phase behavior as flattest as possible in the considered range for the transported reflection phase coefficient. In Fig.3.9 this behavior has been shown.

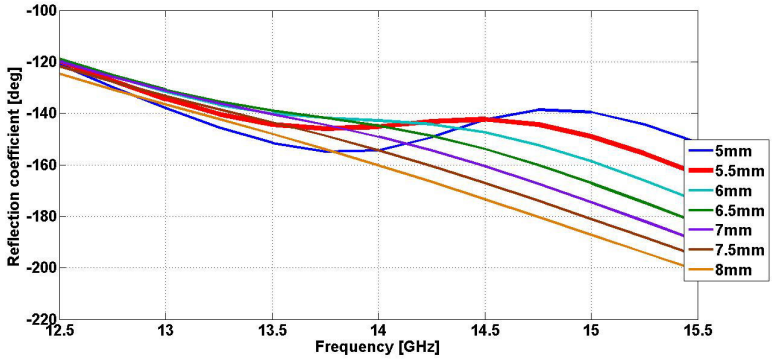


**Fig. 3.9.** Reflection coefficient phase transported near ground plane, varying the varying the dimension of the patches in the first array

Observing the curves in Fig. 3.9, is observed how, while distance between arrays determines the frequency at which phase reversion is performed, the distance between patches of the first array mainly determines the slope of the phase behavior, and, consequently, the bandwidth of the cavity. In the

example, is shown how the curve characterizing a patch length $L_1 = 5.5mm$, achieves an extremely flat behavior in the range $[13.5 - 14]GHz$, while for a value of patch length which tends to the period of the elementary cell $D$ (distance between adjacent patches tending to zero), the transported reflection coefficient tends to the natural phase decreasing like one can observe in a classical PEC sheet (see, in example the curve for $L_1 = 8mm$). Similar aspects can be observed when a variation of the patches of the second array is performed. Maintaining the values found above, a tuning of the patch size of the second array has been done, showing the results in Fig. 3.10.

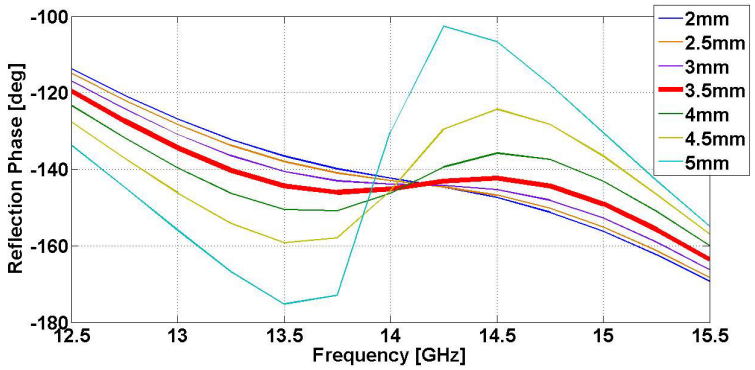


**Fig. 3.10.** Reflection coefficient phase transported near ground plane, varying the varying the dimension of the patches in the second array

In this case, the best value achieved has been obtained for a patch size of the second array $L_2 = 3.5mm$, for small values there are no significant effects of phase reversing, while, for $L_2$ tending to the value $L_1$ regressive phase slope assumes an extremely high value, which is not useful for widening the bandwidth of a Fabry Perot Cavity Antenna. The last optimization have to be operated to the distance $h_1$ , in order to achieve a transported phase reflection of exactly 180 in proximity of the ground plane, respecting the appropriate resonant conditions which leads to constructive interference. So, passing from a value $h_1 = 10.7mm$ to a value $h_1 = 11.7mm$, the curve of the phase reflection near ground plane becomes the one shown in Fig. 3.11.

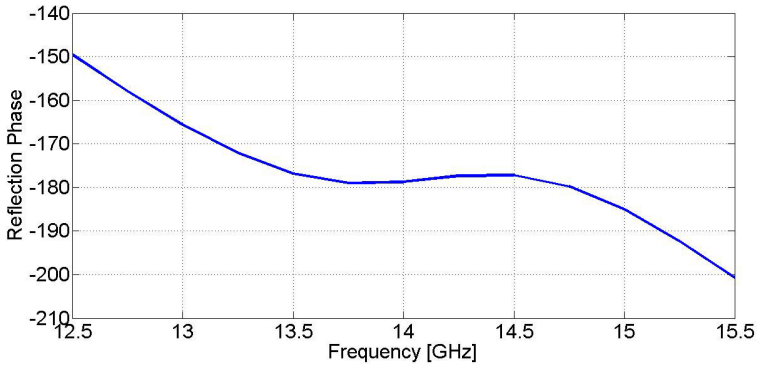


**Fig. 3.11.** Fig. 4. Reflection coefficient phase near the ground plane after optimization

In this case an anomalous constant phase reflection has been achieved in the range between 13.5GHz and 14.5GHz, a relative wideband result if compared to classic metamaterial implementations (in example bulky left handed metamaterials based on split ring resonators and thin wires combination). The useful bandwidth, if considering a total phase variation $\Delta\phi_r \pm 5$, is profusely larger than 10% of the central frequency, and several times larger than classical configurations, thus validating the synthesis technique proposed.

## 3.4 Compact and Wideband Fabry-Perot Cavity Antenna

### 3.4.1 Geometry

After the analysis proposed in Section 3.3, a complete FEM simulation has been carried out, using Ansoft HFSS, in order to integrate the designed double layer surface in a complete Fabry Perot Cavity Antenna powered by a waveguide. A mixed order of the basis functions has been chosen in order to give a good interpretation of the two metamaterial sheets without wasting too much time in simulations and strict convergence criteria have been established. A small refinement of all the geometrical parameters (few iterations for each parameter and no significant differences with the ones found above) has been performed directly on the HFSS model , in order to optimize the -3dB bandwidth of the antenna and total directivity . In a first analysis, a standard WR-75 waveguide has been chosen (with frequency range around [10-15] GHz). Total final lateral dimensions are described in Fig. 3.12, in which a profile of the Fabry Perot Cavity Antenna is shown, while a front view of the PRS, seen from the ground-plane, is seen in Fig. 3.13.

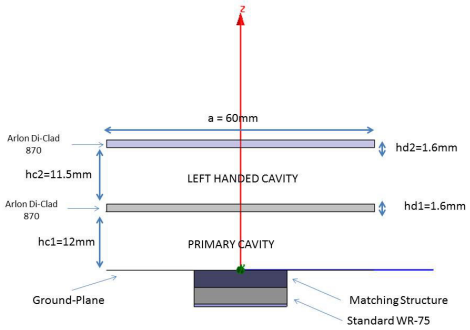


**Fig. 3.12.** Lateral view of the proposed Fabry-Perot Cavity antenna

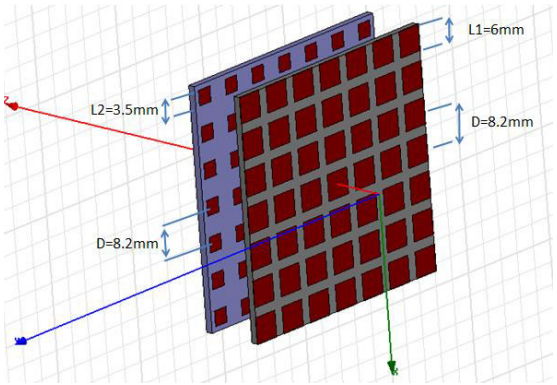


**Fig. 3.13.** Front view, seen from the ground-plane, of the left handed Partially Reflecting Surface

The choose of this waveguide instead of the WR-62 one ([12.4-18] GHz) is justified by the fact that usually Fabry Perot Cavities tend to swiftly deteriorate their behavior at higher frequency respect to the central one, but slowly at the lower frequencies. This general consideration is useful to cover the whole -3dB bandwidth of the antenna with a -10 dB return loss. In effect, finding an optimum coupling between a Fabry Perot Cavity Antenna and a rectangular waveguide is a very difficult step. A rigorous analysis, based on an equivalent circuit model can be provided in [74]. However, a simple analysis of this structure is hard to be carried out due to the complexity of the structure itself and to the fact that equivalent impedances described in [75] cannot be used because the geometrical parameters of the two arrays does not respect the constraints of the model and neglect the reciprocal effects between the

two arrays which cause the useful phase reversing that allow the structure to behave like a left-handed metamaterial.

### 3.4.2 Results

Once completely defined all geometrical parameters of the Wideband Fabry Perot Cavity Antenna, a FEM analysis, varying the height of the waveguide from the standard (using trapezoidal transitions), but maintaining a standard width (horizontal dimension does not affect significantly electrical fields )can be useful to find a good degree of matching between the waveguide and the cavity. A patch antenna is usually used to overcome matching problems , but in this case one wants to obtain a wideband behavior, so techniques used to enlarge patch bandwidth are not so suitable in this context because they waste cross-polar field level, deteriorating the far field behavior or simply because they are not so practical to be designed into a patch inside a cavity. A plot representing return loss at the beginning of the feeding waveguide against the frequency, varying the height of the WR-75, and maintaining the standard value $W = 19.05mm$ for its width, has been performed on the HFSS model and it is shown in Fig. 3.14.

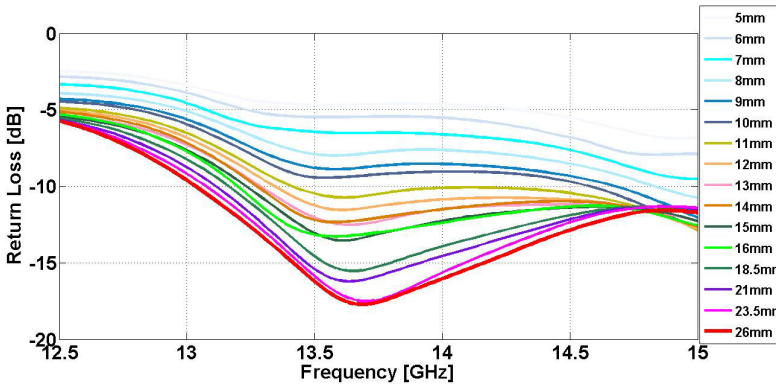


**Fig. 3.14.** Return Loss at the beginning of the feeding waveguide varying its height

A good matching is achieved increasing the cavity height as more as possible, and, for the value h=26mm, the total bandwidth in which the reflected phase transported on the ground plane assumes a value around 180 degrees (see Fig. 3.11) is feed considering a return loss under the threshold of -10dB. So, the total impedance input bandwidth (excluding frequencies out of the constant phase range) is about 13.5 % of the central frequency. However, the most critical aspect to overcome is certainly the -3 dB directivity (in this case, due to the full wave analysis performed one can directly refer to the gain of the antenna) bandwidth, with usually does not exceed few percentage points

(usually less than 1 % in most of configurations). In [70], using this structure on 13 wavelengths large substrates (more than four times bigger than our compact configuration), a bandwidth of 11 % and a directivity of about 20dB was achieved. In Fig. 3.15 is shown the far field components in both planes at the peak frequency of 13.5 GHz.

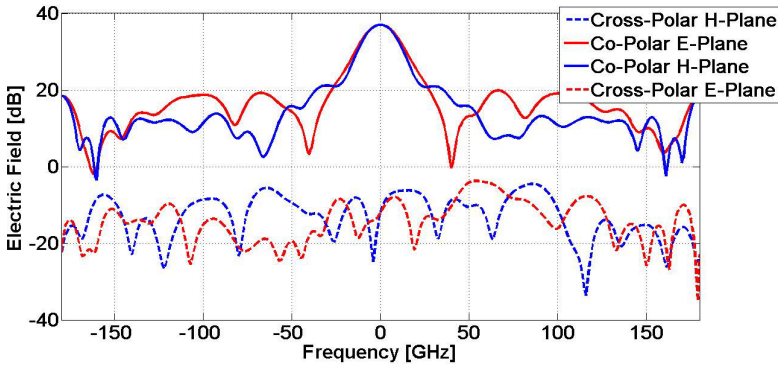


**Fig. 3.15.** Radiation pattern at the peak frequency @13.5GHz

Despite the extreme compactness of the transverse dimensions of the mirrors ( less than 3 wavelength), a very narrow beam is achieved in the main plane of the radiation diagram ( -3dB beam width of about 16 ) and a gain of 19.6dB. In the secondary plane a wider beam is obtained (-3dB beam width of about 20). Secondary lobes are very low and the maximum front-back gain ratio, extremely important for a possible radar application of the antenna, is less than 20dB. Antenna is vertically polarized (in the verse of the waveguide height) and cross-polar field components are appropriately lower than co-polar ones. Other field simulations have been carried out, showing a -3dB bandwidth in an extremely wide range for a Fabry Perot Cavity Antenna (17.5%), going from 12.5GHz up to 15GHz and covering the whole -10dB return loss bandwidth. In order to further validate the wideband behavior of the design, in Fig. 3.16 is shown simulated gain vs frequency at the boresight direction.

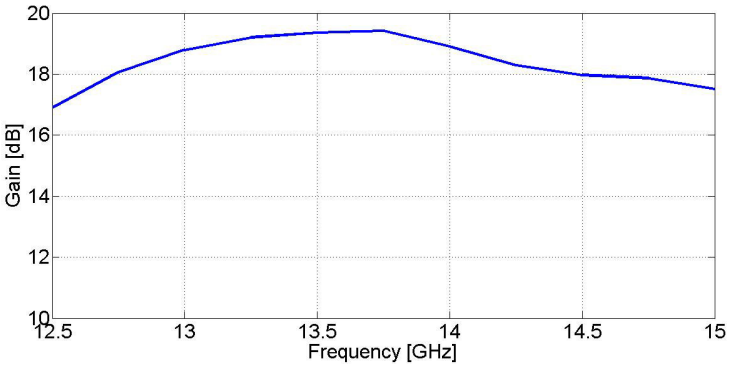


**Fig. 3.16.** Gain at the boresight direction vs frequency

So, taking into account both ranges, the total bandwidth of the antenna is around 13.5%, significantly higher if compared with all other known similar works in literature, especially if related to the extreme compactness of the structure . Radiation pattern on H-plane, for these bandwidth extremes, are both shown in Fig. 3.17.

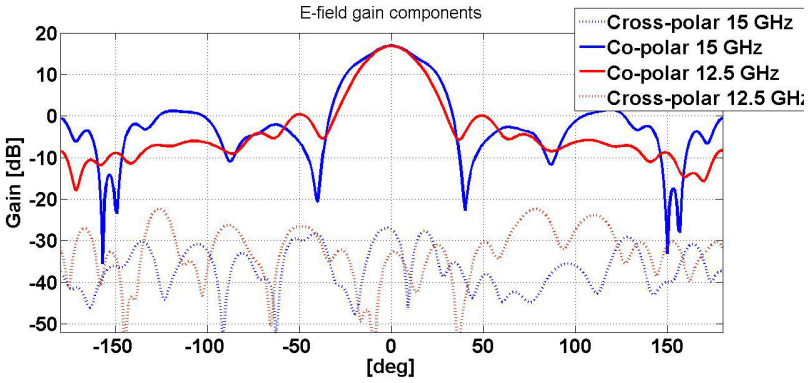


**Fig. 3.17.** Gain patterns on the azimuth plane at the extreme frequency values of the wideband Fabry-Perot Cavity Antenna

It is evident to see how also at bandwidth extremes radiation patterns maintain the same features of the one performed at central frequency, in terms of symmetry, low cross-polarization, high front-back gain ratio and -3dB beam width. A comparison between field components in the elevation plane at 12.5 GHz and 15 GHz, is shown in Fig. 3.18 .

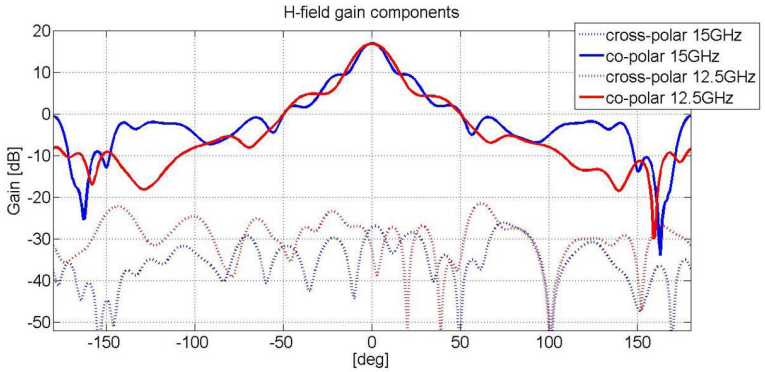


**Fig. 3.18.** Gain patterns on the elevation plane at the extreme frequency values of the wideband Fabry-Perot Cavity Antenna

In this last case, a small enlargement between the two extremes can be seen, but not so evident to prevent the correct functionality of the wideband Fabry Perot Cavity Antenna. So, in conclusion, A wideband Fabry Perot Cavity Antenna, powered by a standard WR-75 waveguide and based on a left handed dual layer structure, has been designed and simulated at the central frequency of 14GHz. The total dimension of the proposed antenna are 60mm x 60mm x 21.5mm, with a volume reduction of several times respect to similar configurations proposed in literature. Total bandwidth is around 13.5% (the highest bandwidth achieved until now for a similar structure, by our knowledge, performed in [70], is around 11%) and the peak gain is 19.6dB (similar to most configurations in literature). Even if a simple procedure has been proposed, a rigorous application of matching between cavity and waveguide [76] could lead to a wider bandwidth, and a mathematical procedure must be developed to easily find all the geometrical parameters by a theoretical way. A simple transverse network could be used to analytically find the fields outside the cavity and a procedure based on applying the paraxial approximation of the wave equation at the radiating surface for analytically finding far field components and to calculate in a rigorous way the fields inside the cavity. Other cavity feeds can be exploited (like wideband and compact slotted antennas) to improve the input impedance bandwidth and this structure could be used for a bandwidth enlargement of other typical narrow-band antennas(like reflectarray antennas).

# 4

# Conclusions

The problem of narrow bandwidth in microstrip antenna configuration has been faced in this work. The main goal, infact, was to introduce into literature new examples of microstrip antennas with wideband behavior, mainly suitable for radar applications. So, a new structure,developed properly modifying microstrip U-slot patch antenna (called Modified U-Slot Antenna ), has been designed, fabricated and tested into the Microwave Laboratory at University of Calabria. Two prototypes, the first one working in P-Band and the second one in C-Band have been developed and tested. Simulations and measures show a wideband behavior, around 20% respect the central frequency, without sacrificing other important features, like gain, around 7 dB for the single element, low cross-polarization level,sensitively enhanced respect to the classic U-Slot configuration and compactness. In particular a 50 % size reduction has been achieved respect to classical microstrip rectangular patch antenna. In order to minimize current which cause cross-polarization, a particular slot shape has been designed and a mathematical method based on empirical formulas has been carried out in order to find in a easy way the optimum value of all geometrical parameters once central frequency and substrate permittivity are fixed. So, in conclusion, a novel design technique, particularly suitable for radar antennas, has been proposed and experimentally validated. In order to further validate this concept in a real system, three prototypes based on this design, but with simplified features respect to the original work (namely Ring Slotted Microstrip Patch Antennas ), have been developed. The first prototype, working in L-Band, has been integrated into a Software Defined Radar for the Landslide Early Warning System proposed in the project $PON01-01530$, while the second one and the third one, working respectively around 450MHz and 900 MHz, have been integrated in a Multimode Multifrequency Airborne Radar system, developed by the Italian research team CORISTA and financed by Italian Space Agency. In both case, in spite of the simplified design, similar behavior to the Modified U-Slot Antenna originally proposed, have been achieved, with successful results for both antenna measurements and outdoor tests of the complete systems. In

particular, outdoor tests, near University of Calabria, have been performed for the Software Defined System integrating the L-Band antenna array, while Airborne radar, integrating P-Band prototypes, has been validate trough two flight campaign carried out by CORISTA. In particular the prototype working at 900 MHz used for the airborne radar, represent a novel dual-polarized configuration, which works with a good isolation between vertical and horizontal polarization, further validating the versatility of the proposed design. The last part of the work has been dedicated to the bandwidth improvement of another structure widely used in radar antenna design, the Fabry Perot Cavity Antenna. Starting with the same goals of the part of the work dedicated to microstrip patch antennas, a wideband Fabry Perot Cavity Antenna composed by two metasurfaces layer has been designed and simulated using the Commercial Software HFSS. A novel ad-hoc synthesis, based on the contemporary employment of Equivalent Transmission Line technique, Method of Moments and propagation analysis by Parabolic Approximation of the Wave Equation in an open resonator, has been proposed in order to design a cavity mirror which performs an anomalous constant phase reflection in a wide range, thus improving the extremely narrow bandwidth operations of classical Fabry Perot Cavity Antenna. A prototype, working in Ku frequency band, with a 13.5 % bandwidth, enhanced gain and low cross-polar level, has been proposed in the final part of this work. Also in this case, like the modified U-Slot Antenna and its simplified version, a very simple and compact structure has been obtained, with enhanced characteristics but, at the same time, extremely practical to design and fabricate. A future extension of this work could be represented by a deeper investigation on the behavior of the Modified U-Slot Antenna Proposed, trying to further improve gain and bandwidth, and finding more rigorous equation for the design. For the last part of the work, new metasurfaces, made up by different patterns, could be considered as cavity mirrors to achieve a wideband behavior of a Fabry Perot, maintaining the same design technique here proposed. An interesting point to develop may be represented by finding analytic equations relating the parameters of the metasurfaces not only to the reflection coefficient phase causing wideband behavior, but also to the input Return Loss and especially to the radiation pattern in both E-Plane and H-Plane.

## References


1. J. R. James, Handbook of microstrip antennas , IEE Electromagnetic Waves Series, 28, 1988.
2. S. Costanzo, I. Venneri, G. Di Massa, and G. Amendola, Hybrid array antenna for broadband millimeter-wave applications, Progress in Electromagnetics Research, Vol. 83, 173183, 2008.
3. S. Costanzo, I. Venneri, and G. Di Massa, Wideband hybrid array concept for millimeter-wave applications, J. Infrared, Millimeter and Terahertz Waves, Vol. 30, No. 4, 374380, 2009.
4. S. Costanzo, F. Venneri, and G. Di Massa, Bandwidth enhancement of aperture-coupled reflectarrays, Electronics Letters, Vol. 42, No. 23, 13201322, 2006.
5. F. Venneri, S. Costanzo, G. Di Massa, and G. Amendola, Aperturecoupled reflectarrays with enhanced bandwidth features, J. Electromagn. Waves Applicat., Vol. 22, No. 11-12, 15271537, 2008.
6. F. Venneri, S. Costanzo, and G. Di Massa, Bandwidth behavior of closely spaced aperture-coupled reflectarrays, Int. Journal of Antennas and Propagat., Article ID 846017, 11 pages, doi:10.1155/2012/846017, 2012.
7. F. Caminita, S. Costanzo, G. Di Massa, G. Guarnieri, S. Maci, G. Mauriello, and I. Venneri, Reduction of patch antenna coupling by using a compact EBG formed by shorted strips with interlocked branch-stubs, IEEE Antennas Wireless Propagat. Letters, Vol. 8, 811814, 2009.
8. S. Costanzo, G. A. Casula, A. Borgia, G. Montisci, I. Venneri, G. Di Massa, and G. Mazzarella, Synthesis of slot arrays on integrated waveguides, IEEE Antennas Wireless Propagat. Letters, Vol. 9, 962965, 2010.
9. S. Costanzo, Synthesis of multi-step coplanar waveguide-to-microstrip transition, Progress in Electromagnetics Research, Vol. 113, 111126, 2011.
10. K. L. Wong, Compact and broadband microstrip antennas , Wiley, 2002.
11. T. Huynh, K.-F. Lee, Single-layer single-patch wideband microstrip antenna, Electronics Letters, Vol. 31, No. 16, 13101312, 1995.
12. K. F. Tong, K. M. Luk, K.-F. Lee, and R. Q. Lee, A broadband Uslot rectangular patch antenna on a microwave substrate, IEEE Trans. Antennas Propagat., Vol. 48, No. 6, 954960, 2000.
13. K. F. Lee, S. L. S. Yang, A. A. Kishk, and K. M. Luk, The versatile Uslot patch antenna, IEEE Antennas Propagat. Magazine, Vol. 52, No. 1, 7188, 2010.

14. K. F. Lee, K. M. Luk, K. M. Mak, and S. L. S. Yang, On the use of U-slots in the design of dual- and triple-band patch antennas, IEEE Antennas Propagat. Magazine, Vol. 53, No. 3, 6073, 2011.
15. K. F. Lee, S. L. S. Yang, and A. A. Kishk, Dual-and multiband Uslot patch antennas, IEEE Antennas Wireless Propagat. Letters, Vol. 7, 645647, 2008.
16. K. F. Tong, and T.-P.Wong, Circularly polarized U-slot antenna, IEEE Trans. Antennas Propagat., Vol. 55, No. 8, 23822385, 2007.
17. M. Clenet, and L. Shafai, Multiple resonances and polarization of Uslot patch antenna, Electronics Letters, Vol. 35, No. 2, 101103, 1999.
18. S. Wiegand, G. H. Huff, K. H. Pan, and J. T. Bernhard, Analysis and design of broad-band single-layer rectangular U-slot microstrip patch antennas, IEEE Trans. Antennas Propagat., Vol. 51, No. 3, 457468, 2003.
19. S. Costanzo, G. Di Massa, Near-field to far-field transformation with planar spiral scanning, Progress in Electromagnetics Research, Vol. 73, 4959, 2007.
20. S. Costanzo, G. Di Massa, Far-field reconstruction from phaseless near-field data on a cylindrical helix, J. Electromagn. Waves Applicat., Vol. 18, 10571071, 2004.
21. S. Costanzo, G. Di Massa, Direct far-field computation from bipolar near-field samples, J. Electromagn. Waves Applicat., Vol. 20, 11371148, 2006.
22. S. Costanzo, and G. Di Massa, An integrated probe for phaseless nearfield measurements, Measurement, Vol. 31, 123129, 2002.
23. S.H. Chou, J.H. Lu, Cross-Polarization Level Reduction of Broadband Triangular Patch Antenna With Dual L-Strip Lines, Microwave And Optical Technology Letters, Vol. 33, No. 4, pp. 300-303, May 2002
24. H.W. Lai, K.M. Luk ,Design and Study of Wide-Band Patch Antenna Fed by Meandering Probe, IEEE Transactions On Antennas And Propagation, Vol. 54, No. 2, pp. 564-571, February 2006
25. G.H. Huff, J.T. Bernhard, Improvements in the performance of microstrip antennas on finite ground planes through ground plane edge serrations, IEEE Microwave and Wireless Components Letters, Vol.12, Issue 8, pp. 308 310, Aug. 2002.
26. H. Wang, X.B Huang, D.G. Fang, A Novel Corner-Fed Patch to Reduce Cross-Polarization for a Microstrip Antenna Array, APMC 2008, pp. 1-4, Macau, Dec. 2008
27. S. Costanzo, A. Costanzo, Compact slotted antenna for wideband radar applications, Advances in Intelligent Systems and Computing, Vol. 206, 989996, 2013.
28. S. Costanzo, A. Costanzo, Compact U-slotted antenna for broadband radar applications, Journal of Electrical and Computer Engineering, Article ID 910146, 2013.
29. D. D. Grieg, H. F. Englemann, " Microstrip, a new transmission technique for the kilomegacycle range," Proceedings of IRE Vol.40, No.12,1644-1650, December 1952.
30. G. A. Deschamp, Microstrip Microwave Antennas, 3rd USAF Symp. on Antennas, 1953
31. E. V. Byron, A new flush-mounted antenna element for phased array application, Proc. Phased-Array Antenna Symp.,187-192, 1970
32. R. E. Munson, Single slot cavity antennas assembly, U.S. Patent No. 3713 162, Jan. 23, 1973.

33. F. Jolani, A. M. Dadgarpour, Compact M-slot folded antenna for WLAN, Progress In Electromagnetics Research Letters, Vol. 3, 3542, 2008
34. A. J. Ansari, P. Singh, S. K. Dubey, R. U. Khan,B. R. Vishvakarma, H-shaped stacked patch for dual-band operation, Progress In Electromagnetics Research B, Vol. 5, 291302, 2008
35. A. J. Ansari, S. K. Dubey,P. Singh, "Analysis of U-slot loaded Patch for Dual-band Operation, International Journal of Microwave and Optical Technology", Vol. 3, No.2 ,80-84, 2008
36. A. C. Balanis," Antenna Theory, Analysis and Design, 2nd Edition" ,John Wiley & Sons Inc., 1997
37. P. S. Hall, Probe compensation in thick microstrip patches, Electronics Letters, vol. 23, no. 11, pp. 606607, 1987.
38. S. Costanzo, F. Spadafora, A. Borgia, H. O. Moreno, A. Costanzo and G. Di Massa, "High Resolution Software Defined Radar System for Target Detection", Journal of Electrical and Computer Engineering, Volume 2013 (2013), Article ID 573217, 2013
39. G. Aloi, A. Borgia, S. Costanzo, G. Di Massa, V. Loscr, E. Natalizio, P. Pace, F. Spadafora, Software Defined Radar: synchronization issues and practical implementation, COGART, International Conference on Cognitive Radio and Advanced Spectrum Management, Barcelona, 2011.
40. C. Prathyusha, S. N. Sowmiya, S. Ramanathan, R. Soman, K.P. Amrita, V. V. Deepthi, M. Chinnam, J. Nandhini, Implementation of a low cost synthetic aperture radar using software defined radio, International Conference on Computing Communication and Networking Technologies (ICCCNT), Karur, India ,2010.
41. M. Fuhr, M. Braun, C. Sturmz, L. Reichardtz, F. K. Jondral , An SDR-based Experimental Setup for OFDM-based Radar, 7th Karlsruhe Workshop on Software Radio Karlsruhe, Germany, March 2012.
42. H. Hellsten, L. M. Ulander, A. Gustavsson, and B. Larsson, Development of VHF CARABAS II SAR, Proc. SPIE Radar Sensor Technology, 2747, pp. 48-60, 1996.
43. E. G. Njoku, W. J. Wilson, S. H. Yueh, S. J. Dinardo, F. K. Li; T. J. Jackson, V. Lakshmi, J. Bolten, Observations of soil moisture using a passive and active low-frequency microwave airborne sensor during SGP99, IEEE Trans. Geosci. Remote Sens., vol.40, no.12, pp. 2659-2673, 2002.
44. G. Smith-Jonforsen, L. M H Ulander, L. Xianyun Low VHF-band backscatter from coniferous forests on sloping terrain, IEEE Trans. Geosci. Remote Sens., vol.43, no.10, pp.2246-2260, 2005.
45. L. M. H. Ulander, M. Lundberg, W. Pierson, and A. Gustavsson, Change detection for low-frequency SAR ground surveillance, IEE Proc. Radar, Sonar and Navigation, vol. 152, no. 6, pp. 413-420, 2005.
46. R. Scheiber, P. Prats, F. Hlire, Surface Clutter Suppression Techniques for Ice Sounding Radars: Analysis of Airborne Data, Proc. of EUSAR 2008, Friedrichshafen, Germany, June 2008.
47. K. Jezek, S. Gogineni, X. Wu, E. Rodriguez, F. Rodriguez-Morales,A. Hoch, A. Freeman, and J. Sonntag, Two-frequency radar experiments for sounding glacier ice and mapping the topography of the glacier bed, IEEE Trans. Geosci. Remote Sens., vol. 49, no. 3, pp. 920929, Mar. 2011.
48. C. Fabry, A. Peròt," Theorie et Applications d'une Nouvelle Method de Spectroscopie Interferentielle", Ann Chim. Phys., Vol. 16, pp.115-143, 1899.

49. G. V. Trentini,"Partially reflecting sheet arrays", IRE Trans Antennas Propagation 4, pp. 666-671, 1956.
50. T. Tamir, "Leaky-Wave Antennas," in Antenna Theory, R. E. Colin and F. J. Zucker Eds., ed New York, McGraw Hill, 1969.
51. A. A. Oliner, "Leaky-Wave Antennas," in Antenna Engineering Handbook, R. C.Johnson, Ed., ed New York: McGraw Hill, 1993.
52. D. R. Jackson and N. G. Alexopoulos, Gain enhancement methods for printed circuit antennas, IEEE Trans. Antennas Propag., vol. 33 , pp. 976987, Sept. 1985.
53. H. Y. Yang and N. G. Alexopoulos, Gain enhancement methods for printed circuit antennas through multiple superstrates, IEEE Trans. Antennas Propag., vol. 35, pp. 860863, July 1987.
54. V. G. Veselago, The electrodynamics of substances with simultaneously negative values of $\epsilon$ and $\mu$ , Usp. Fiz. Nauk, vol. 92, pp. 517-526, 1967.
55. 10. J. B. Pendry, A. J. Holden, D. J. Robbins and W. J. Stewart, Magnetism from Conductors and Enhanced Nonlinear Phenomena, IEEE Trans. Microwave Theory Tech, Vol. 47, No. 11, pp. 2075-2084, November 1999
56. D. Sievenpiper, L. Zhang, F. Jimenez Broas, N. G. Alexopulos, and E. Yablonovitch, High-impedance electromagnetic surfaces with a forbidden frequency band, IEEE Trans. Microwave Theory Tech. vol. 47, pp. 2059-2074.
57. M. Thvenot, C. Cheype, A. Reineix, and B. Jecko, Directive Photonic Bandgap Antennas, IEEE Trans. Microwave Theory Tech., vol. 47, pp. 21152122, Nov. 1999.
58. C. Cheype, C. Serier, M. Thevenot, T. Monediere, A. Reinex, and B. Jecko, An electromagnetic bandgap resonator antenna, IEEE Trans. Antennas Propag., vol. 50, no. 9, pp. 12851290, Sep. 2002.
59. A. R. Weily, L. Horvath, K. P. Esselle, B. C. Sanders, and T. S. Bird, A planar resonator antenna based on a woodpile EBG material, IEEE Trans. on Antennas Propag., vol. 53, no. 1, pp. 216223, Jan. 2005.
60. H.-Y. D. Yang, N. G. Alexopoulos, and E. Yablonovitch, Photonic band-gap materials for high-gain printed circuit antennas, IEEE Trans. Antennas Propag., vol. 45, pp. 185187, Jan. 1997.
61. B. Temelkuaran, M. Bayindir, E. Ozbay, R. Biswas, M. M. Sigalas, G. Tuttle, and K. M. Ho, Photonic crystal-based resonant antenna with a very high directivity, J. Appl. Phys., vol. 87, pp. 603605, 2000.
62. G. Poilasne, P. Pouliguen, J. Lenormand, K. Mahdjoubi, C. Terret, and P. Gelin, Theoretical study of interactions between antennas and metallic photonic bandgap materials, Microwave Opt. Technol. Lett., vol. 15, pp. 384389, 1997.
63. R. Gardelli, M. Albani, F. Capolino, "Array Thinning by Using Antennas in a FabryPerot Cavity for Gain Enhancement", IEEE Trans. on Antennas Propagation,vol. 54, n.7, pp. 1979-1990, 2006.
64. A. P. Feresidis and J. C. Vardaxoglou, High Gain Planar Antenna Using Optimised Partially Reflective Surfaces, IEE Proc. Microwave Antennas Propagation, vol. 148, pp. 345-350, December 2001
65. M. Caiazzo, S. Maci, N. Engheta, " A Metamaterial Surface for Compact Cavity Resonator" IEEE Antennas and Wireless Propagation Letters, vol. 3, pp. 261-264, 2004
66. P. Feresidis, G. Goussetis, S. Wang and J.C Vardaxoglu, "Artificial Magnetic Conductor Surfaces and Their Application to Low-Profile High-Gain Planar

Antennas", IEEE Trans. Antennas Propag., vol. 53 no 1 , pp. 209215, Jan. 2005.
67. G. Goussetis, P. Feresidis, J.C Vardaxoglu, "Tailoring the AMC and EBG Characteristics of Periodic Metallic Arrays Printed on Grounded Dielectric Substrate",IEEE Trans. Antennas Propag., vol. 54 no 1 , pp. 8289, Jan. 2006.
68. C. Mateo-Segura, M. Garcia-Vigueras, G. Goussetis, J.L. Gomez-Tornero, A. Feresidis, " Analysis of sub-wavelength cavity leaky-wave antennas with high-impedance surfaces" Antennas Propagation Conference, Loughborough, 2009.
69. Y. Sun, Z. Ning Chen, Y. Zhang, H. Chen, "Subwavelength Substrate-Integrated Fabry-Prot Cavity Antennas Using Artificial Magnetic Conductor", IEEE Trans. Antennas Propag., vol. 60 no. 1 , pp. 30-35, Jan. 2012.
70. C. Mateo-Segura, A. P. Feresidis, and G. Goussetis, "Bandwidth Enhancement of 2-D Leaky-Wave Antennas With Double-Layer Periodic Surfaces",IEEE Trans. Antennas Propag., vol. 62 no. 2 , pp. 586-593, Feb. 2014.
71. N. Wang, Q. Liu, C. Wu, L. Talbi, Q. Zeng, and J. Xu, "Wideband Fabry-Perot Resonator Antenna With Two Complementary FSS Layers",IEEE Trans. Antennas Propag., vol. 62 no. 5 , pp. 2463-2472, May 2014.
72. M.A. Leontovich , V.A.Fock, "Investigation of Radio Wave Propagation", ed. B.A. Vendeski, AN SSSR, Moskow, pp.13-39, 1948.
73. G. Di Massa, O.H. Moreno, S. Costanzo, Simplified Model of a Fabry-Perot Antenna, 7th European Conference on Antennas and Propagations, Goteborg 2013.
74. O. Luukkonen, C. Simovski, G. Granet, G. Goussetis, D. Lioubtchenko, A. V. Raisanen, S. A. Tretyakov, Simple and Accurate Analytical Model of Planar Grids and High-Impedance Surfaces Comprising Metal Strips or Patches, IEEE Transactions on Antennas and Propagations, Vol. 56, pp. 1624-1632, June 2008.
75. F.Venneri, S.Costanzo, G. di Massa, G. Amendola, Aperture-Coupled Reflectarrays with Enhanced Bandwidth Features, J. of Electromagne Waves and Appl., Vol.22, pp. 1527-1537, 2008.
76. O. Bucci, G. Di Massa, Open resonator powered by rectangular waveguide, IEE Proceedings-H, Vol. 139, pp.323-329, 1992

# 5

# Publications

### *Journals*

1. S. Costanzo, A. Costanzo, Compact Modified U-Slot Patch Antenna (MUSA) with Reduced Cross-Polarization, IEEE Antennas and Propagation Magazine, in press, 2014.

2. S. Costanzo, F. Spadafora, G. Di Massa: A. Borgia, A. Costanzo, G. Aloi, P. Pace, V. Loscr, H. Moreno, Potentialities of USRP-Based Software Defined Radar Systems, Progress In Electromagnetics Research B, Vol. 53, pp 417-435, 2013.

3. S. Costanzo, A. Costanzo: "Compact U-Slotted Antenna for Broadband Radar Applications", Journal of Electrical and Computer Engineering, Special Issue on Advances in Radar Technologies, L. Ed. S. Costanzo, 2013.

4. S. Costanzo, F. Spadafora, A. Borgia, H. Moreno, A. Costanzo, G. Di Massa: High Resolution Software Defined Radar System for Target Detection, Journal of Electrical and Computer Engineering, Special Issue on Advances in Radar Technologies, L. Ed. S. Costanzo, 2013.

5. S. Costanzo, G. Di Massa, A. Costanzo, A. Borgia, C. Papa, G. Alberti, G. Salzillo, G. Palmese, D. Califano, L. Ciofanello, M. Daniele, C.Facchinetti, F. Longo, R. Formaro: "Multimode/Multifrequency Low Frequency Airborne Radar Design", Journal of Electrical and Computer Engineering, Special Issue on Advances in Radar Technologies, L. Ed. S. Costanzo, 2013.

6. A. Costanzo, S. Costanzo, G. Di Massa, Design of a new broadband slot-loaded patch antenna, Atti della Fondazione Giorgio Ronchi, Anno LXVII, n.2, pp. 225-230, 2012.

### *Conferences*

1. S. Costanzo, A. Costanzo, Compact Slotted Antenna for Wideband Radar Applications , Advances in Intelligent Systems and Computing Volume 206, pp 989-996, 2013.

2. S. Costanzo, F. Spadafora, A. Borgia, H. Moreno, A. Costanzo, G. Di Massa, High Resolution Software Defined Radar System for Target Detection , Advances in Intelligent Systems and Computing Volume 206, pp 997-1005, 2013.

3. S. Costanzo, A. Costanzo, Compact Slotted Antenna for Wideband Radar Applications , World Conference in Information Technology, World CIST 13, Algarve, Portugal, March 2013.

4. S. Costanzo, F. Spadafora, A. Borgia, H. Moreno, A. Costanzo, G. Di Massa, High Resolution Software Defined Radar System for Target Detection , World Conference in Information Technology, World CIST 13, Algarve, Portugal, March 2013.

5. S. Costanzo, A. Costanzo, Modified U-Slot Patch Antenna with Low Cross Polarization for Broadband Application , XIX Riunione Nazionale Elettromagnetismo, Roma, Settembre 2012.

6. S. Costanzo, G. Di Massa, F. Spadafora, A. Raffo, A. Borgia, A. Costanzo, L. Morrone, " Radar Activity at University of Calabria ",XXI Riunione Nazionale Elettromagnetismo, Padova, September 2014.

7. S.Costanzo, A. Costanzo," Slotted Patch Antenna with Low Cross-Polarization ", European Conference on Antennas and Propagation, EuCAP 2014, The Hague, April 2014.

8. S. Costanzo, G. Di Massa, F. Spadafora, A. Raffo, A. Costanzo, L. Morrone, P.D Moreno, A. Borgia, Radar System for Landslides Monitoring , Mediterranean Meeting on Monitoring, Modelling, Early Warning of Extreme Events Triggered by Heavy Rainfall, Rende, June 2014.